applied mechanics

MDPI

Article

Numerical and Geometric Analysis of Side-Wall Inclination Angle Effects on Longitudinal Hat-Stiffeners in Steel Plates

Guilherme Garcia Madsen [1], Mariana Alvarenga Alves [2], Luiz Alberto Oliveira Rocha [1,2], Elizaldo Domingues dos Santos [1,2], William Ramires Almeida [1] and Liércio André Isoldi [1,2,*]

[1] School of Engineering, Federal University of Rio Grande—FURG, Rio Grande 96201-900, Brazil; guilhermegarciamadsen@furg.br (G.G.M.); luizrocha@furg.br (L.A.O.R.); elizaldosantos@furg.br (E.D.d.S.); walmeida@furg.br (W.R.A.)

[2] Graduate Program in Computational Modeling (PPGMC), Federal University of Rio Grande—FURG, Rio Grande 96201-900, Brazil; mariana.alves@furg.br

* Correspondence: liercioisoldi@furg.br; Tel.: +55-53-99109-7356

Abstract

Thin steel plates with stiffeners are widely employed in several branches of engineering, combining mechanical strength with low weight and serving as both structural and cladding components. However, the influence of the side-wall inclination angle of hat-stiffeners on the stiffness distribution and deflection patterns of steel plates remains insufficiently explored. This study conducts computational modeling to evaluate the deflection of thin steel plates reinforced with hat-stiffeners. The plates were considered simply supported and subjected to a uniformly distributed load. The Constructal Design method and the exhaustive search technique were employed, allowing for geometric evaluation and optimization. A fraction corresponding to 30% of the plate volume was removed and redistributed to generate longitudinal hat-stiffener geometries by varying its side-wall angle and thickness. The smaller base of the hat-stiffeners was imposed as a geometric constraint and therefore kept fixed. The results indicate a nonlinear trend between the side-wall angle, the moment of inertia, and the resulting deflection, leading to a new geometrical pattern that connects the angular inclination to the overall stiffness behavior of the plate. Angles between 105° and 130° provided the best performance, reducing the maximum deflection by 93.72% compared with the reference plate and improving it by around 7.5% relative to previous studies. These findings illustrate how geometric configuration can enhance performance in line with Constructal Design principles.

Keywords: hat-stiffened plates; structural analysis; computational solid mechanics; out-of-plane displacements; Constructal Design

check for updates

Received: 14 September 2025
Revised: 13 October 2025
Accepted: 16 October 2025
Published: 20 October 2025

Citation: Madsen, G.G.; Alves, M.A.; Rocha, L.A.O.; dos Santos, E.D.; Almeida, W.R.; Isoldi, L.A. Numerical and Geometric Analysis of Side-Wall Inclination Angle Effects on Longitudinal Hat-Stiffeners in Steel Plates. *Appl. Mech.* **2025**, *6*, 78. https://doi.org/10.3390/applmech6040078

Copyright: © 2025 by the authors. Licensee MDPI, Basel, Switzerland. This article is an open access article distributed under the terms and conditions of the Creative Commons Attribution (CC BY) license (https://creativecommons.org/licenses/by/4.0/).

1. Introduction

Metal plates are widely employed in several branches of engineering, typically serving both structural and cladding functions. The addition of stiffeners to these plates provides unique advantages in terms of structural efficiency and design, as it significantly increases strength while keeping the overall structural weight relatively low. Stiffened plates are commonly used in aerospace, marine, and civil engineering structures [1–5]. Various stiffener geometries exist, each imparting distinct characteristics to the mechanical behavior of the plate. In this study, the hat-stiffener type is adopted, as illustrated in Figure 1a. Figure 1b shows an application employing hat-stiffeners in an aircraft fuselage section.

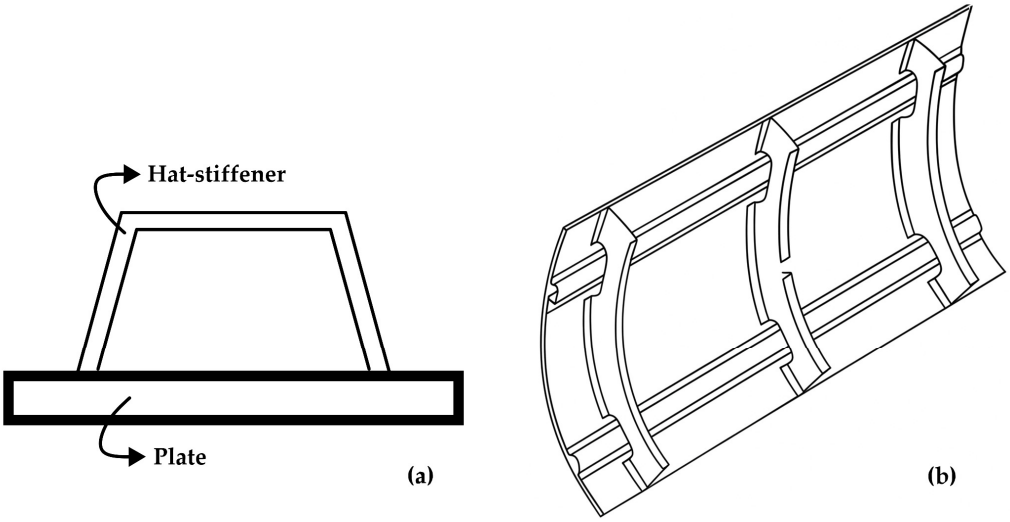


Figure 1. Hat-stiffened plates: (**a**) a cross-sectional view and (**b**) application in an aircraft fuselage.

Regarding the manufacturing of stiffened plates, the connection between the stiffener and the plate can be achieved through several joining methods, depending on the material type, the intended application, and the applicable design codes and standards. For metallic structures, conventional joining techniques such as welding and riveting are commonly employed [6–9]. The stiffeners themselves can be produced through different manufacturing processes, including profile extrusion or, in the specific case of hat-stiffeners, by sheet metal-forming operations such as stamping or bending [10–12].

Among the approaches to analyzing these structural components, computational modeling offers significant potential for simulating plates reinforced with hat-stiffeners, as it enables the development of different combinations of stiffener geometric parameters and the investigation of their effects. The Finite Element Method (FEM) has been extensively employed in studies of stiffened plates [13–15] and implemented in commercial software such as ANSYS and ABAQUS. Regarding the development of different combinations of stiffener geometric properties, the Constructal Design method, proposed by Adrian Bejan in 1996 [16–20], has proven to be an effective tool for geometric analysis in structural engineering problems [21–23]. This method is based on the Constructal Law, which states the following: "For a finite-size system to remain in operation, its geometric configuration must evolve continuously in order to provide the best flow access for currents flowing through the system" [16–20,24]. Bejan and Lorente [18] applied this concept to structural engineering, establishing that structures function as minimum-volume connections, allowing stresses to "flow" from one component to its neighbor, and that the most efficient use of material occurs when the maximum allowable stresses are uniformly distributed throughout the structure. It should be emphasized that for the Constructal Design method to be applied, it is necessary to define design variables and constraints. Furthermore, to investigate the influence of variations in the design variables and to identify the best geometry, appropriate performance indicators must be established [16–20,24,25].

The Constructal Design method has been employed for the development and evaluation of different stiffener geometries installed on plates subjected to bending through numerical simulation. Troina et al. [26] minimized the central deflection of plates subjected to bending due to a distributed load by optimizing I-type stiffeners of equal height, arranged both transversely and longitudinally. Similarly, Nogueira et al. [27] also minimized the maximum and central deflections of plates with I-type stiffeners but considering stiffeners of different heights. Furthermore, Pinto et al. [28] and Kucharski et al. [29] extended the analysis by simultaneously evaluating the maximum deflection and the von Mises

stress in stiffened plates, demonstrating that the Constructal Design approach can enhance both stiffness and stress distribution efficiency through geometric evolution. Additionally, Lima et al. [30] applied the same methodology to investigate the elasto-plastic buckling of stiffened plates under uniaxial compression, confirming the potential of Constructal Design to improve the ultimate buckling performance of metallic structures.

In the field of stiffened plate analysis with hat-stiffeners, Tharian and Nandakumar [31,32] conducted a numerical investigation using the FEM and highlighted that hat-stiffeners exhibit higher torsional rigidity and a superior strength-to-weight ratio compared with open-section stiffeners, thereby demonstrating their structural superiority. Pal et al. [33] performed a numerical analysis of two plate configurations: one reinforced with hat-stiffeners and the other with I-type (flat) stiffeners. Boundary conditions and stiffener dimensions were varied while maintaining a constant volume, and the results indicated that the hat-stiffened plate exhibited smaller displacements. Virág and Szirbik [34] employed modal analysis to identify and eliminate vibration frequencies that could cause damage in a hat-stiffened plate. Tharian and Nandakumar [31] also carried out a structural analysis of bunkers and proposed a superelement formulation that reduces the computational cost of numerical analyses of hat-stiffened plates. Filippatos et al. [35] improved the efficiency of aerospace components incorporating hat-stiffeners. Raju et al. [36] investigated damage occurrence in ship structures made of composite materials reinforced with hat-stiffeners. More recently, using the Constructal Design method, Alves et al. [22,23] evaluated different longitudinal and transverse hat-stiffener geometries while keeping the side-wall inclination angle constant and identified the most effective configuration for reducing the deflections of a plate subjected to a distributed load.

In addition, several recent studies on hat-stiffened panels have predominantly focused on composite materials, exploring structural performance under various loading and environmental conditions. Sun et al. [37] developed FEM–Artificial Neural Network (ANN) hybrid approaches to predict the buckling and ultimate loads of composite hat-stiffened panels under in-plane shear, while Kumar et al. [38] proposed the Constrained Variational Asymptotic Method (C-VAM) to efficiently capture nonlinear buckling and delamination effects. Optimization-based analyses by Kumar et al. [39] and Kumar et al. [40] examined weight reduction, spacing, and geometric parameters, identifying closed-section stiffeners as optimal configurations for stiffness-to-weight improvement. Experimental validations by Kumar et al. [41], Kumar et al. [42], and Wang et al. [43] confirmed the strong agreement between FEM predictions and laboratory tests, especially for axial and edge compression scenarios.

In turn, interface and environmental effects have also been examined: Lei et al. [44] demonstrated that temperature and humidity significantly reduce bonding strength, whereas Liu and Guan [45] showed that inserting fillers in deltoid regions increases local stiffness and modifies failure modes. Complementary analytical contributions by Qiu [46] introduced equivalent stiffness formulations for simplified design assessments.

Given the relevance of hat-stiffened plates, this study proposes a geometric analysis and optimization of steel plates with longitudinal hat-stiffeners, simply supported and subjected to a uniformly distributed load. The Constructal Design method, combined with the exhaustive search technique, is employed with emphasis on varying the side-wall inclination angle of the stiffener while maintaining a constant material volume. The analysis of the generated configurations is carried out through a numerical model using the FEM, aiming to identify the configuration that minimizes the maximum deflection. To initiate the application of the Constructal Design method, a reference plate without stiffeners is adopted, and 30% of its volume is redistributed into stiffeners. To do so, the thickness of the reference plate is reduced, and stiffeners are generated by keeping the width of the

smaller base constant while varying the side-wall inclination angle. Using a reference plate with dimensions of 2000 mm × 1000 mm, configurations with one to five hat-stiffeners can be generated, with thicknesses ranging from 4.75 mm to 12.7 mm. The computational model was developed via the FEM using the ANSYS Mechanical APDL 2024 R2 software package, with the SHELL281 finite element. One can note that the present investigation is an extension of the work previously published by Alves et al. [22].

It is worth emphasizing that in addition to the works already discussed, several other studies [47–57] have further explored the mechanical behavior of hat-stiffened plates made of composite materials, whereas thin steel plates with hat-stiffeners remain a relatively underexplored topic in the literature. This observation highlights the scientific motivation of the present study, which focuses on the geometric optimization of thin steel plates with hat-stiffeners and aims to extend the Constructal Design approach to metallic structures.

In summary, although recent advances have improved the understanding of hat-stiffened panels, almost all previous investigations considered the side-wall angle as a fixed geometric parameter. No systematic evaluation of this variable has been reported, especially for metallic plates. In contrast, the present work investigates the influence of side-wall angle under constant material volume, unveiling nonlinear correlations between the side-wall angle, the moment of inertia, and the resulting deflection. Thus, this study fills an important gap by linking the geometric evolution of the stiffener cross-section to the overall stiffness behavior, thereby broadening the Constructal Design framework for application to thin steel hat-stiffened plates.

2. Materials and Methods

2.1. Materials

Regarding material selection, this study adopts ASTM A36 [58] structural steel as a representative material to analyze the structural behavior of plates with hat-stiffeners, due to its wide range of applications in the civil, naval, and offshore industries, which employ stiffened plates to enhance strength and reduce structural weight. ASTM A36 structural steel provides a balanced combination of mechanical strength, weldability, availability, and cost, making stiffened plates fabricated from this steel a suitable choice for specific applications. Its relevance is demonstrated in naval applications, where it is used in hulls, decks, and bulkheads; in offshore platform modules; and in civil engineering, where this steel is employed in stiffened plates for bridge components, slabs, and floors, with stiffeners enhancing load-bearing capacity, controlling displacements, and reducing weight [23].

2.2. Methods

The application of the Constructal Design method requires the definition of local and/or global constraints. These constraints serve as limits for the variation in the defined degrees of freedom, generating multiple geometries and, ultimately, the definition of performance indicators, which can be maximized or minimized to improve the obtained results. It is important to emphasize, however, that the Constructal Design is not an optimization method per se but rather a tool for geometric evaluation. Therefore, to perform the optimization process, the Constructal Design method must be combined with an optimization technique, such as the exhaustive search method. In this context, during the geometric evaluation and optimization process, the Constructal Design method generates the search space (possible geometric configurations given the constraints and degrees of freedom), while the exhaustive search identifies the geometry that provides the best results [25]. To improve the understanding of the relationship between the stages of this work, Figure 2 presents the methodological framework.

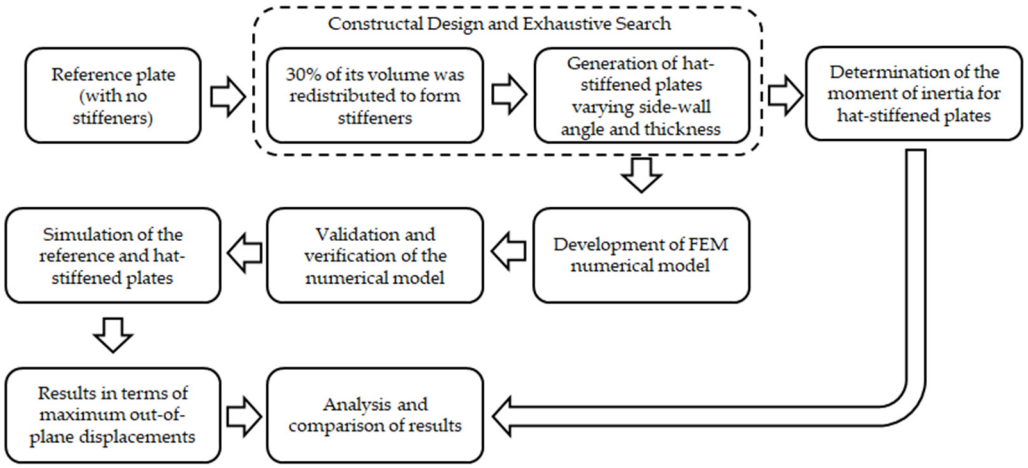


Figure 2. Methodological framework of this study.

In practical structural engineering applications, stiffened plates are supported along their edges, a condition that does not restrict rotational movement at the supports. This feature can be observed in ship deck structures, bridge panels, and steel slabs [23]. To reflect this condition in numerical simulations, the adopted boundary condition considers the plate as simply supported along its edges, i.e., vertical displacements are restrained, while rotations are allowed at the support points.

In the present study, the mechanical behavior of the generated configurations was investigated using the Finite Element Method (FEM) implemented via the commercial software ANSYS Mechanical APDL (version 2024 R2, ANSYS Inc., Canonsburg, PA, USA). The selected finite element was SHELL281, illustrated in Figure 3, which is suitable for the simulation of thin to moderately thick plates. This finite element has eight nodes and six degrees of freedom per node, consisting of three translations (U_x, U_y, and U_z) and three rotations (θ_x, θ_y, and θ_z) [59]. The SHELL281 finite element was adopted for both the plate and the hat-stiffeners, as in previous works [21–23,27]. In the FEM, displacements must be determined to obtain deflections, which are computed through the matrix manipulation of a system of algebraic equations [1,60,61]. To ensure that the computational model is correctly defined, validations and verifications were performed by comparing the results with references reported in the literature.

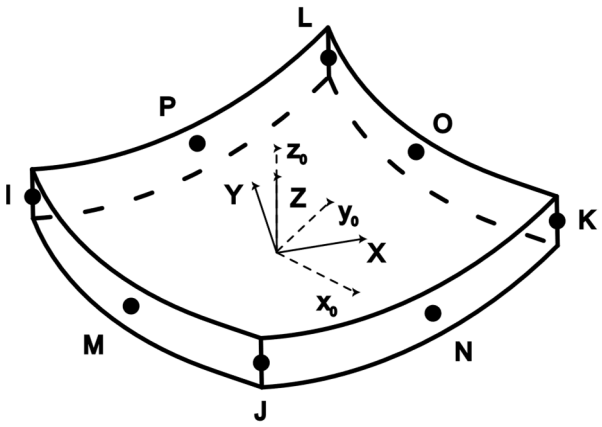


Figure 3. SHELL281 finite element.

As previously mentioned, the application of the Constructal Design method begins with a reference plate, 30% of whose volume will be transformed into stiffeners. The dimensions of the reference plate are as follows: width a = 2000 mm; length b = 1000 mm; and thickness t_{rp} = 20 mm. Considering a and b as fixed constraints, the 30% volume fraction

is removed from its thickness t_{rp} [21,23,26,27] and converted into stiffeners, resulting in plates with a thickness of t = 14 mm in which the hat-stiffeners are installed. It should be noted that this is not a material reduction but rather a redistribution (from the thickness of the reference plate to the stiffeners); hence, the total steel volume remains unchanged.

As stated earlier, the material adopted is ASTM A36 structural steel, with a Young's modulus E = 200 GPa and Poisson's ratio ν = 0.3 [62,63]; this material has also been employed in previous studies [21,23,26,27]. Regarding boundary conditions, a uniformly distributed load of 10 kPa was applied; this load level was chosen to ensure that the plate remains within the linear elastic regime [21,23,26,27]. The edges were considered simply supported, as explained earlier, reflecting practical structural engineering applications. Figure 4 presents a schematic drawing of the plate with two hat-stiffeners. The choice of hat-stiffener thickness was based on the commercially available plate thicknesses that could be used to fabricate these stiffeners. Therefore, the following values were adopted: t_s = 4.75 mm (3/16 in); t_s = 6.35 mm (1/4 in); t_s = 8.00 mm (5/16 in); t_s = 9.53 mm (3/8 in); and t_s = 12.7 mm (1/2 in). The stiffener side-wall angle θ_s was varied from 75° to 150° in increments of 5°. The width of the smaller base was fixed at b_t = 40 mm. Using these parameters, by selecting the plate thickness and varying the side-wall inclination angle, other geometric parameters such as the stiffener height and larger base width were determined, generating multiple geometric configurations.

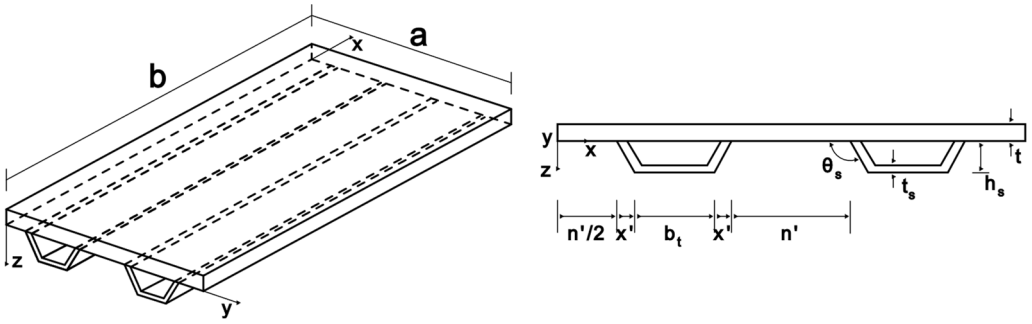


Figure 4. Schematic representation of the plate with two hat-stiffeners.

Considering that the analyzed plates could be joined with other plates in a practical application, the distance from the stiffener to the plate edge was set as half of the distance between the stiffeners on the plate. Figure 4 shows an example with two stiffeners, where n' represents the distance between the stiffeners, and $n'/2$ represents the distance from the stiffener to the plate edge. In the case of a single stiffener, it was centered along the longer dimension of the plate.

Based on the defined spacing and obtained dimensions, cases with one to five hat-stiffeners placed on the plate were analyzed. The dimensions used for each geometric configuration of the plate and stiffeners, as well as the results in terms of the maximum deflection for each analyzed configuration, are presented in Appendix A, through Tables A1–A5, organized by case. As can be observed in Appendix A, in some cases, certain geometric configurations had to be discarded due to physical interference between the stiffeners.

The moment of inertia of the geometries was determined as follows. Initially, the geometric centroid was obtained. Subsequently, the moment of inertia with respect to this centroid was evaluated for the external contour of the geometry, neglecting the hollow (void) region, as illustrated in Figure 5a. Thereafter, the moment of inertia associated with the centroid of the hollow region, depicted in Figure 5b, was computed and subtracted from the previously obtained value. In this manner, the effective moment of inertia of the adopted geometry was established, as shown in Figure 5c.

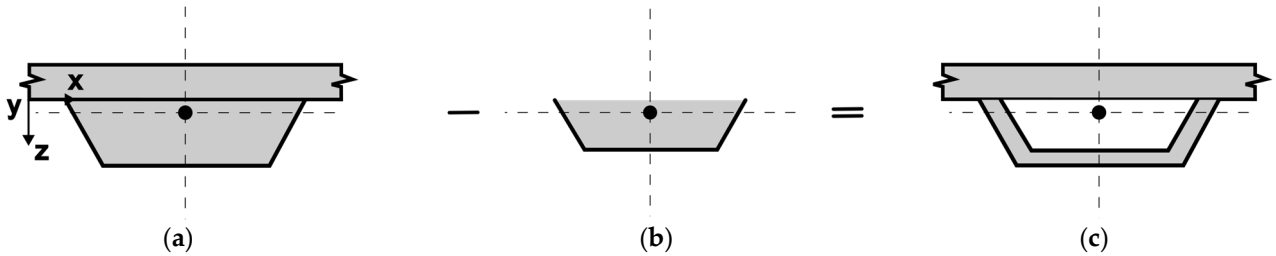


Figure 5. The procedure for determining the moment of inertia of each obtained geometry: (**a**) using the external contour of the section, disregarding the internal void; (**b**) computing the moment of inertia associated with the void region; and (**c**) subtracting the moment of inertia of the void from that of the external contour.

In summary, computational modeling was conducted in ANSYS APDL using the SHELL281 finite element, under linear elastic and static conditions. The non-stiffened reference plate (2000 mm × 1000 mm × 20 mm) and the hat-stiffened plates (2000 mm × 1000 mm × 14 mm) were considered as simply supported on all edges and subjected to a uniformly distributed pressure of 10 kPa. The material adopted corresponds to ASTM A36 steel, with a Young's modulus of 200 GPa and Poisson's ratio of 0.3. A structured quadrilateral mesh was used, and a mesh convergence analysis defined an element size of 10 mm, ensuring the independence of the numerical results from the spatial discretization. In total, 336 geometric configurations for hat-stiffened plates were simulated, combining variations in the number of longitudinal stiffeners (1 to 5), in the stiffener thickness (4.75 mm, 6.35 mm, 8.00 mm, 9.53 mm, and 12.7 mm), and in the side-wall inclination angle (75°, 90°, 105°, 120°, 135°, and 150°), maintaining a constant total volume equivalent to 30% of the reference plate redistributed into the stiffeners. The maximum displacement was numerically defined for each configuration, supporting the Constructal Design and Exhaustive Search procedures applied in this study.

3. Results

3.1. Results of Validation and Verification of Computational Model

The validation and verification procedures presented herein aim to ensure the accuracy of the proposed computational model and have been previously employed in [22,23].

Starting with model validation, a numerical simulation was developed based on an experimental study conducted by Carrijo et al. [64]. This study aimed to evaluate the maximum central deflection of a plate with I-stiffeners, illustrated in Figure 6a. A uniformly distributed load of 0.96 kPa was applied to the stiffened plate, with simple supports applied at its four corners. The mechanical properties of the material used are as follows: E = 2.5 GPa and ν = 0.36. In the simulation, a regular converged mesh was adopted, consisting of square SHELL281 finite elements with an edge length of 2.436 mm. Figure 6b presents the distribution of out-of-plane displacements obtained from the numerical model. The experimental results obtained by Carrijo et al. [64] indicated a central deflection of U_z = 6.2200 mm. The numerical model predicted a central deflection of U_z = 6.5075 mm.

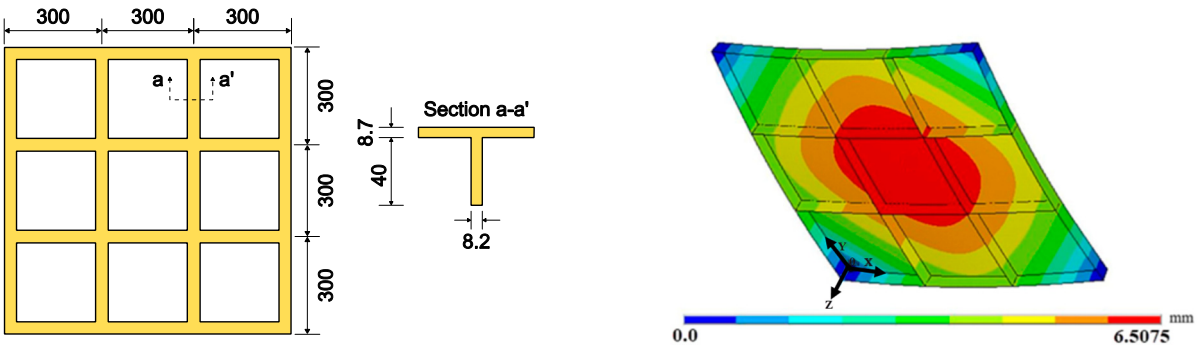


Figure 6. Computational model validation: (**a**) schematic illustration of stiffened plate tested experimentally (in mm); (**b**) distribution of deflections obtained from proposed numerical model.

Subsequently, two computational model verifications were performed considering simply supported stiffened metallic plates. In the first case, the plate with two hat-stiffeners, modeled by Tharian and Nandakumar [32], which used the SHELL63 and SHELL93 finite elements, was reproduced using the SHELL281 finite element. The results, in terms of the maximum deflections, were compared. The geometric characteristics of the plate can be seen in Figure 7. The material used was steel, with properties E = 210 GPa and ν = 0.3. The loading consisted of a uniformly distributed load of 10 kPa.

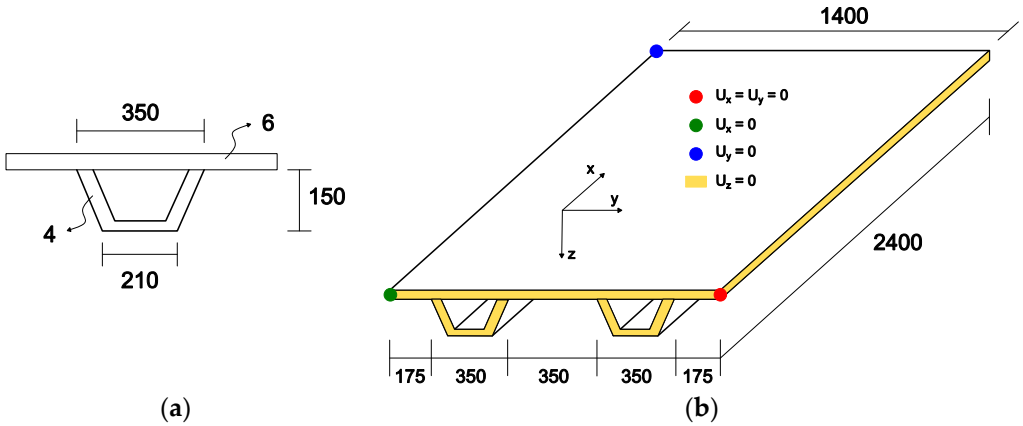


Figure 7. First computational model verification: (**a**) stiffener details (in mm); (**b**) plate details (in mm) and boundary conditions.

The performed mesh convergence test together with the results from Tharian and Nandakumar [32] are presented in Figure 8. The maximum displacements reported by Tharian and Nandakumar [32] were 0.7198 mm with the SHELL63 element and 0.7214 mm with the SHELL93 element, whereas the proposed model using square SHELL281 elements of 10 mm in a converged mesh yielded 0.7295 mm.

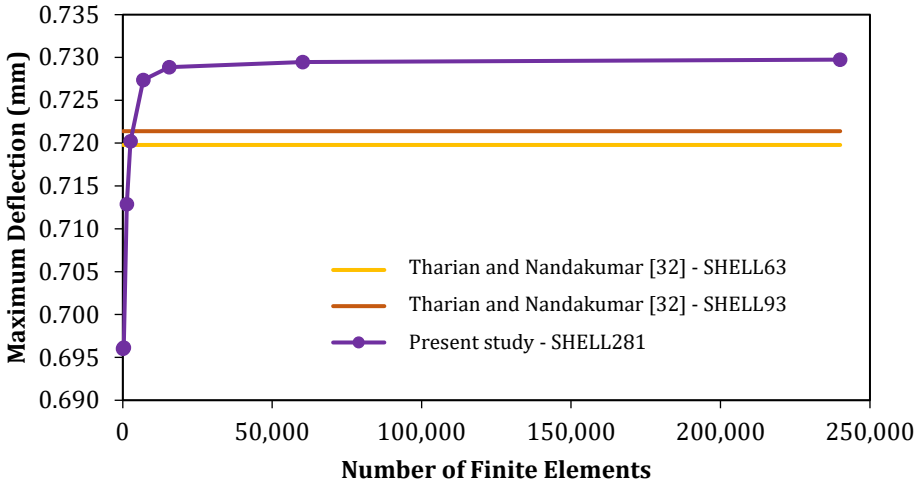


Figure 8. Mesh convergence of the first verification [32].

The second verification considered a plate with a hat-stiffener centered along the longer dimension of the simply supported plate, as shown in Figure 9. Pal et al. [33] analyzed this plate and evaluated 25 hat-stiffener configurations; the simulations were conducted using SHELL181 finite elements for the plate and BEAM3 finite elements for the stiffeners. It is noteworthy that Pal et al. [33] maintained the stiffener volume constant (320,000 mm^3) while generating the 25 configurations, with the dimensions presented in Table 1. The material used for both the plate and the stiffener was steel, with properties E = 200 GPa and ν = 0.3. The plate was subjected to a uniformly distributed load of 1 kPa. Mesh convergence tests were performed considering Case 1 from Table 1, defining a mesh composed of square SHELL281 finite elements with a size of 10 mm for all 25 cases.

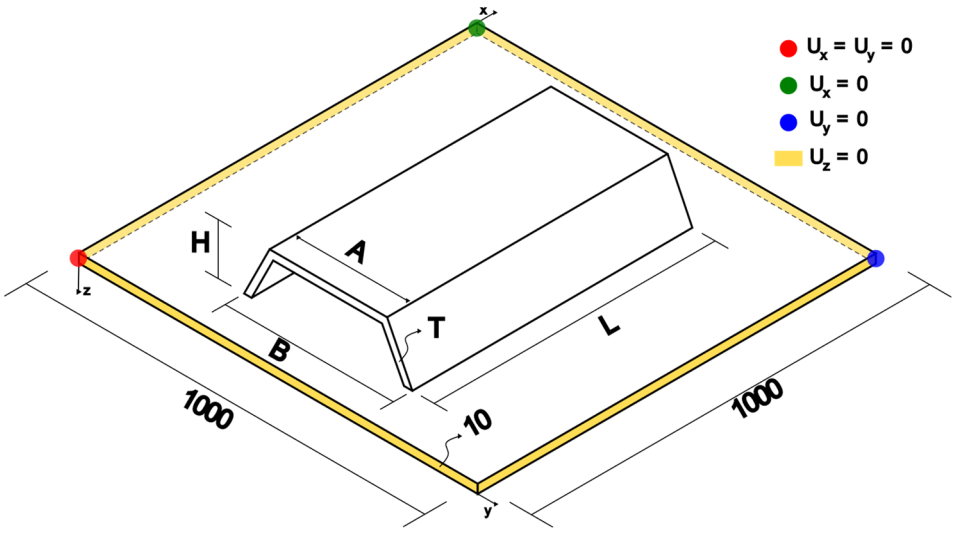


Figure 9. Plate analyzed in second model verification (in mm).

Table 1. The dimensions (in mm, see Figure 9) of the hat-stiffener for the second verification.

Case	Thickness (*T*)	Shorter Base (*A*)	Longer Base (*B*)	Height (*H*)	Length (*L*)
1	2	35	60	65	955.90
2	3	35	60	65	637.26
3	4	35	60	65	477.95
4	5	35	60	65	382.36
5	6	35	60	65	318.63
6	2	40	60	65	932.78
7	3	40	60	65	621.86
8	4	40	60	65	466.39
9	5	40	60	65	373.11
10	6	40	60	65	310.93
11	2	40	65	70	878.09
12	3	40	65	70	585.39
13	4	40	65	70	439.04
14	5	40	65	70	351.23
15	6	40	65	70	292.70
16	2	40	60	70	881.92
17	3	40	60	70	587.95
18	4	40	60	70	440.96
19	5	40	60	70	352.77
20	6	40	60	70	293.97
21	2	35	65	65	950.02
22	3	35	65	65	633.35
23	4	35	65	65	475.01
24	5	35	65	65	380.01
25	6	35	65	65	316.67

The results obtained by Pal et al. [33] and by the proposed numerical model are presented in Figure 10.

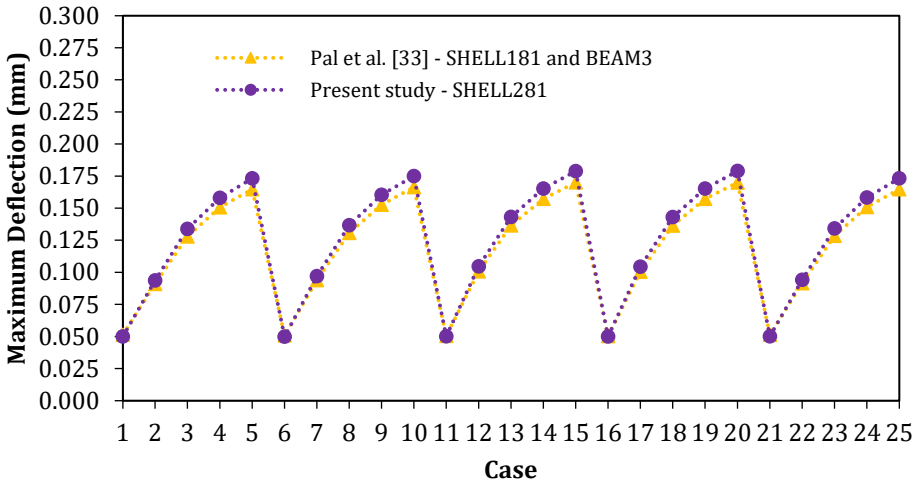


Figure 10. Results for second model verification [33].

3.2. Results of Case Study

As previously explained, all geometric configurations of the longitudinal hat-stiffeners were derived from a reference plate without stiffeners while maintaining three conditions: (i) the total volume of the plates with stiffeners is the same as that of the reference plate without stiffeners, transforming 30% of the reference plate volume into hat-stiffeners but keeping the plate's width and length unchanged; (ii) the angle of the hat-stiffeners' side-walls varied between 75° and 150° in 5° increments, with stiffener thicknesses of 4.75 mm,

6.35 mm, 8.00 mm, 9.53 mm, and 12.7 mm; and (iii) the width of the stiffener's smaller base must be fixed at b_t = 40 mm. Based on these conditions, the use of the Constructal Design method enabled the generation of geometric configurations of plates with one to five longitudinal hat-stiffeners, considering five different hat-stiffener thicknesses.

To determine the appropriate spatial discretization for all simulated hat-stiffened plates, a mesh convergence test was performed on the plate with the most complex geometry, i.e., the one with five hat-stiffeners. As in Alves et al. [22,26], SHELL281 finite elements with a square shape were used, with side lengths varying from 5 mm to 40 mm (M1 = 40 mm; M2 = 30 mm; M3 = 20 mm; M4 = 15 mm; M5 = 10 mm; and M6 = 5 mm). The results are shown in Figure 11, where it can be observed that the maximum plate deflection stabilizes starting from mesh M4. However, to avoid mesh dependency, mesh M5 with 10 mm elements was adopted for all numerical simulations.

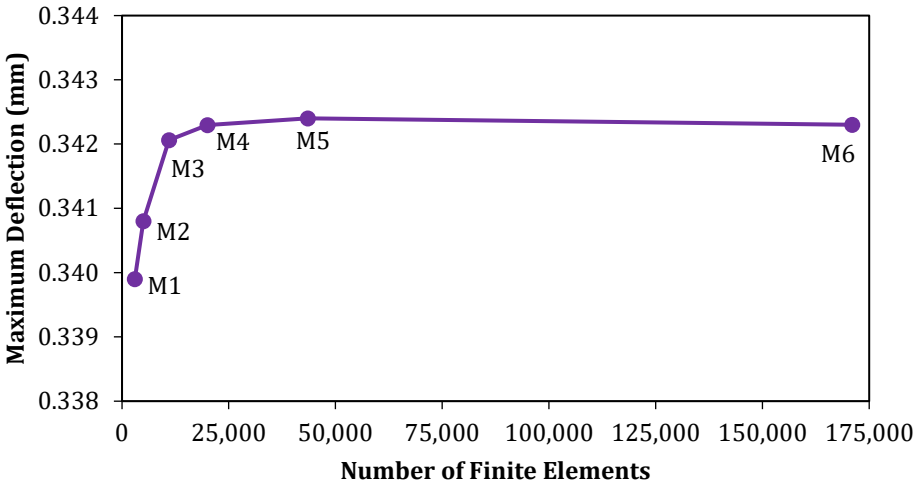


Figure 11. Mesh convergence test of case study.

The main purpose of employing the Constructal Design method by testing the angular variation in the stiffener walls is to enhance structural efficiency. In this study, efficiency is evaluated through the direct comparison of the maximum deflections obtained. Additionally, some results will be compared with the best outcomes reported by Alves et al. [22], who analyzed similar plates; however, in their study, the stiffener wall inclination angle was fixed at 120°, while the stiffener height was varied.

The numerical results obtained in terms of the maximum deflection of the hat-stiffened plates were recorded and are presented in Figures 12–16 for plates with one to five longitudinal hat-stiffeners, respectively. Additionally, the maximum deflection of the reference plate (without stiffeners), U_z = 0.6976 mm, is also plotted in these figures.

For a general comparison, Table 2 presents the best and worst results obtained for each number of hat-stiffeners, including the geometric properties, the relative difference in the maximum deflection obtained in the stiffened plate simulation compared to the reference plate, and the moment of inertia of the structure with respect to the x-axis (see Figure 5).

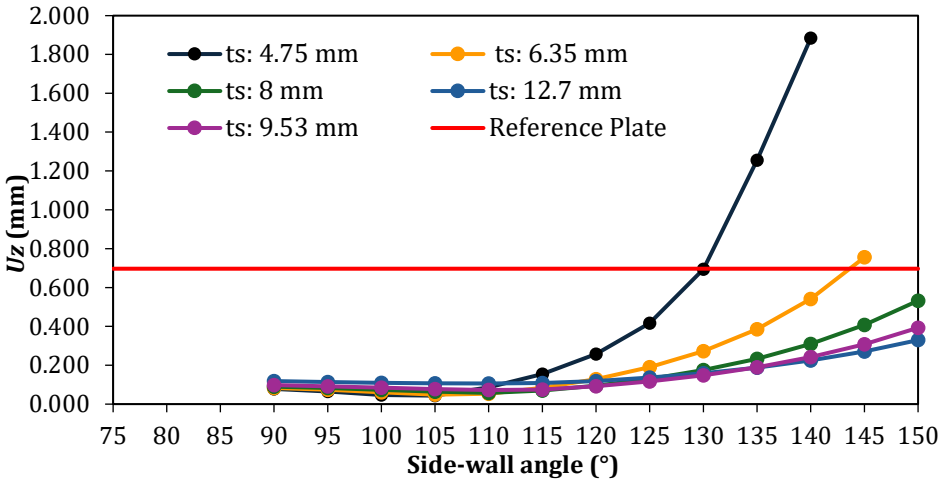


Figure 12. The maximum deflection for the case with a single hat-stiffener.

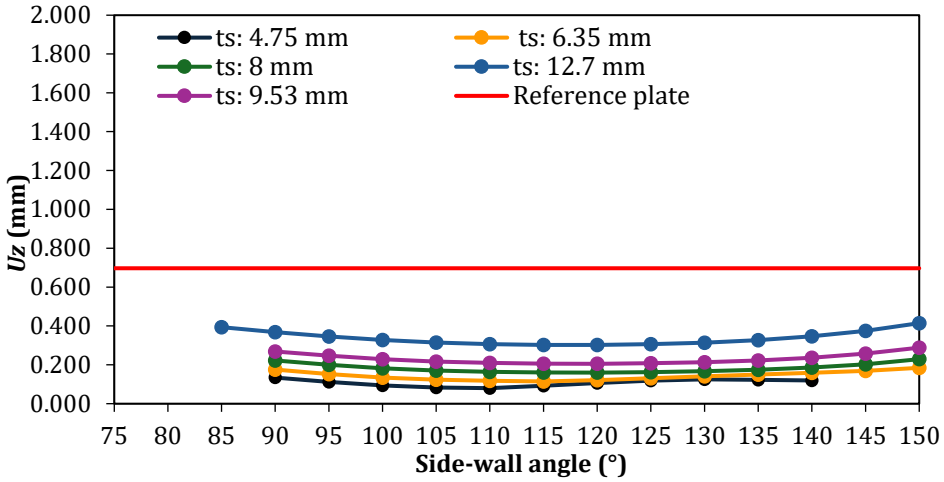


Figure 13. The maximum deflection for the case with two hat-stiffeners.

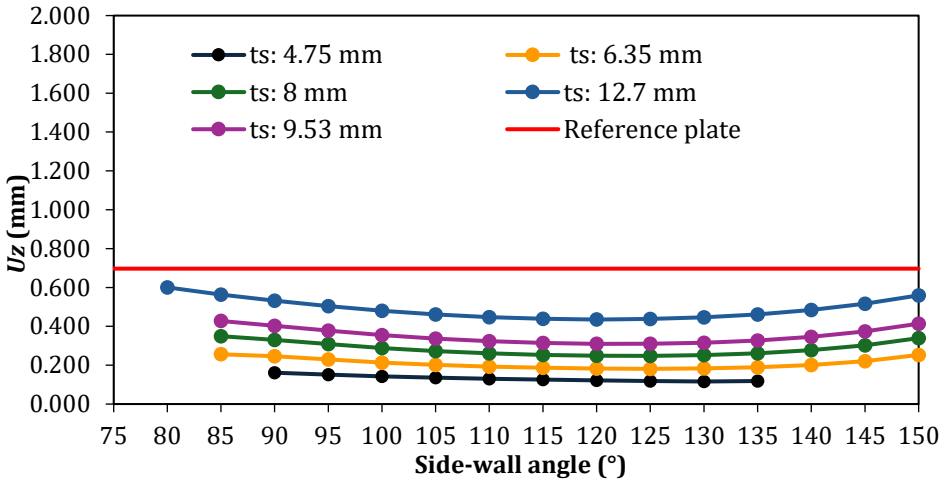


Figure 14. The maximum deflection for the case with three hat-stiffeners.

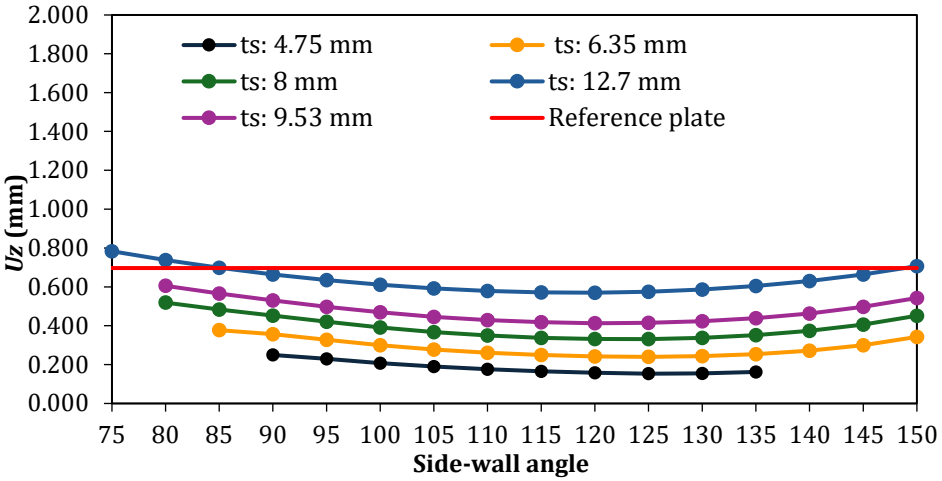


Figure 15. The maximum deflection for the case with four hat-stiffeners.

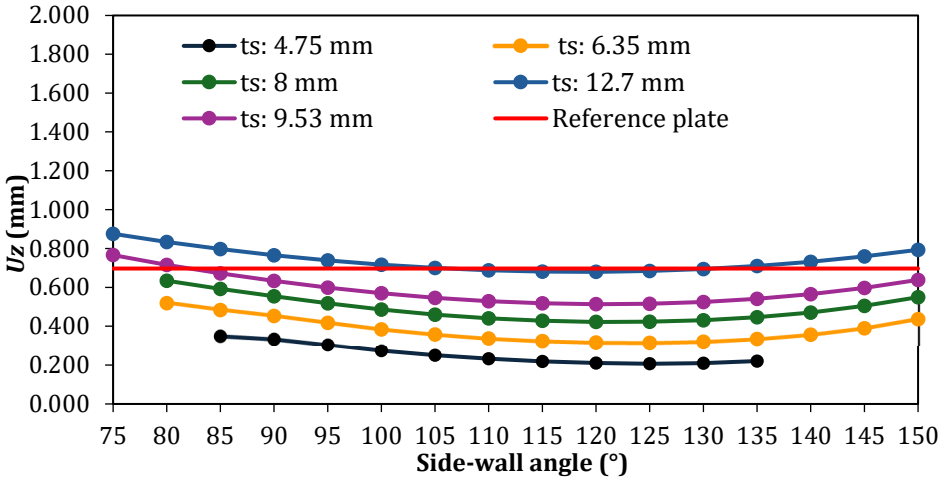


Figure 16. The maximum deflection for the case with five hat-stiffeners.

Table 2. Best and worst results for each number of hat-stiffeners.

Number of Hat-Stiffeners	θ_s (°)	t_s (mm)	h_s (mm)	U_z^{max} (mm)	RD (%) U_z^{max}	I_x (mm^4)
1	105	4.75	590.7399	0.0438	−93.72	5.06×10^9
	140	4.75	393.1154	1.8840	170.08	2.33×10^9
2	110	4.75	277.9512	0.0800	−88.53	1.24×10^9
	150	12.7	49.0551	0.4143	−40.61	3.35×10^7
3	130	4.75	145.9516	0.1163	−83.32	3.78×10^8
	80	12.7	57.8478	0.6005	−13.91	4.84×10^7
4	125	4.75	112.9568	0.1539	−77.94	2.42×10^8
	75	12.7	37.7243	0.7834	12.30	2.17×10^7
5	125	4.75	87.0888	0.2074	−70.27	1.51×10^8
	75	12.7	26.3158	0.8760	25.57	1.21×10^7

4. Discussion

4.1. Discussion of Validation and Verification of Computational Model

The distribution of out-of-plane displacements obtained from the proposed numerical model (see Figure 6b) and the experimental results reported by Carrijo et al. [64] show a relative error of 4.58% between the numerical and experimental data, considering the central

(maximum) deflection. It is important to note that, although there are some differences between this plate and the plate studied in the present work (dimensions, boundary conditions, material, and stiffener type), the numerical simulation of this case allowed for the assessment of whether the model can accurately capture the basic physical behavior of stiffened plates under bending. This serves as a representative validation, supporting the overall reliability of the proposed modeling strategy. Therefore, the computational model can be considered validated through a proof-of-concept approach, which is typically used when an exact experimental baseline is not available.

In turn, as shown in Figure 8, for the first verification of the computational model, using the results of Tharian and Nandakumar [32], the difference between the SHELL281 and SHELL63 elements was 1.35%, and it was 1.12% between the SHELL281 and SHELL93 elements. Both results confirm the validity of the proposed numerical model. In the second verification, the results obtained by Pal et al. [33] and those of the proposed model are as presented in Figure 9. Among all cases, the maximum relative difference was 5%, and the average relative difference was 3.3%, thereby confirming the accuracy of the proposed computational model. From these results, one can infer that the proposed numerical model was properly verified.

4.2. Discussion of Case Study

In general, from Figures 12–16 it can be observed that, in all cases, the minimum deflection occurred when the smallest hat-stiffener thickness (t_s = 4.75 mm) was adopted, while the maximum deflection occurred when the largest hat-stiffener thickness (t_s = 12.7 mm) was employed.

In the cases with a single stiffener (Figure 12), 60 geometric configurations were generated and analyzed. An atypical behavior was identified when compared to the other cases (Figures 13–16). For all adopted t_s values, it was observed that increasing the inclination of the stiffener side-walls initially leads to a reduction in the maximum deflection. However, upon reaching a certain value of θ_s, in plates with smaller t_s, a sharp increase in the maximum deflection occurs. In plates with larger t_s, this effect is less pronounced, presenting a more gradual increase in the maximum deflection. Another important feature is that, for these cases, the sharp increase occurs within specific θ_s values depending on the adopted t_s value: $\theta_s = 105^\circ$ for t_s = 4.75 mm and t_s = 6.35 mm and $\theta_s = 110^\circ$ for t_s = 8.00 mm, t_s = 9.53 mm, and t_s = 12.7 mm. Regarding deflections, one can also note that most geometric configurations exhibited a maximum deflection smaller than that of the reference plate, except for the case with t_s = 4.75 mm and $\theta_s = 120^\circ$, which showed nearly the same out-of-plane displacement, as well as the cases with t_s = 4.75 mm and $\theta_s = 135^\circ$ and 140° and the case with t_s = 6.35 mm and $\theta_s = 145^\circ$. The best result was obtained for t_s = 4.75 mm when the hat-stiffener side-walls have $\theta_s = 105^\circ$, reaching a reduction of 93.72% in the maximum deflection compared to the reference plate.

Figure 17 presents three cases with a single stiffener and t_s = 4.75 mm, allowing for a comparative analysis of the displacement behavior under different inclination angles of $\theta_s = 100^\circ$ (Figure 17a), $\theta_s = 105^\circ$ (Figure 17b), and $\theta_s = 110^\circ$ (Figure 17c). In Figure 17b, the minimum maximum deflection occurred at $\theta_s = 105^\circ$, since this geometry provided the best balance between the length of the larger base ($b_t + 2y'$) and the dimension n', resulting in a more uniform displacement distribution and the second highest moment of inertia among the cases with one stiffener (see Table A1). In contrast, Figure 17a shows the case with $\theta_s = 100^\circ$, where, despite having the greatest moment of inertia, displacement concentrations are observed in regions outside the stiffener (length n'). Finally, Figure 17c illustrates the configuration with $\theta_s = 110^\circ$, where a more pronounced displacement concentration shift to the region within the stiffener.

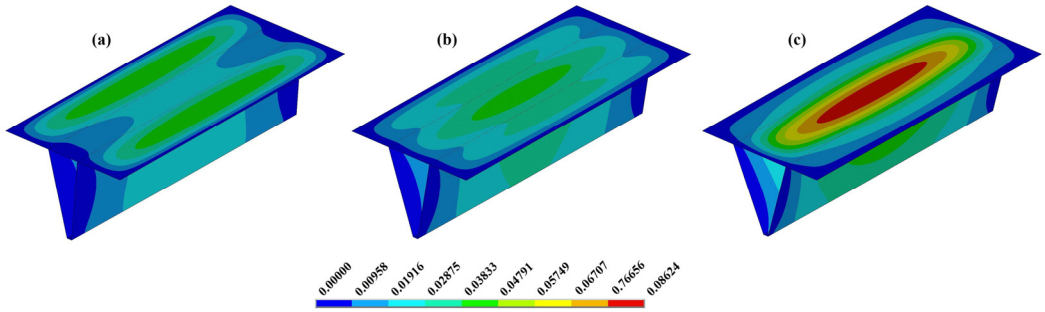


Figure 17. Strain distribution for plates with one hat-stiffener, t_s = 4.75 mm, and the following stiffener side-wall angles: (**a**) θ_s = 100°; (**b**) θ_s = 105°; and (**c**) θ_s = 110°.

The analysis of the results presented in Table 2 indicates that the plate with one hat-stiffener (Case 1), a side-wall angle of θ_s = 105°, and a thickness of t_s = 4.75 mm achieved the best performance, resulting in a relative difference of −93.72% compared to the reference plate. As additional stiffeners are added, the performance tends to decrease, reaching −70.27% for the case with five hat-stiffeners.

For the remaining t_s values in the single hat-stiffener cases, a similar trend was observed: the configuration yielding the smallest maximum deflection is also characterized by one of the highest moments of inertia, generally associated with an angle of 105° (when t_s = 6.35 mm) or 110° (when t_s = 8.0 mm, t_s = 9.53 mm, and t_s = 12.7 mm).

By adding another stiffener to the plate, the cases with two stiffeners are obtained, with the results shown in Figure 13, resulting in 64 geometric configurations being generated and analyzed. The variation in the inclination angle of the hat-stiffener side-walls initially caused a decrease in the maximum deflections; however, upon reaching specific θ_s values, an increase in the maximum deflection occurred. The θ_s values where the change in behavior occurs are θ_s = 110° for t_s = 4.75 mm; θ_s = 115° for t_s = 6.35 mm; and θ_s = 120° for t_s = 8.00 m, t_s = 9.53 mm, and t_s = 12.7 mm. Here, a trend analogous to that of the single-stiffener cases is observed, with the three largest thicknesses producing the best results at the same side-wall angle. Furthermore, the configurations with t_s = 4.75 mm displayed a distinct response: following the change in trend and the subsequent increase in the maximum deflection, a slight stabilization was observed around θ_s = 130°. This stabilization suggests that, beyond θ_s = 130°, the geometry reaches a balance that restrains further displacement growth. In addition, and as in the single-stiffener investigation, all geometric configurations exhibited maximum deflections below those of the reference plate, contributing to improved structural performance. The best results were obtained for t_s = 4.75 with a side-wall angle of θ_s = 110°, representing a reduction of 88.53% in the maximum deflection compared to the reference plate. Figure 18 presents the results for t_s = 4.75 mm at side-wall angles θ_s = 105° (Figure 18a), θ_s = 110° (Figure 18b), and θ_s = 115° (Figure 18c). One can note that the geometric configuration generated at θ_s = 110° (Figure 18b) exhibited the best displacement distribution.

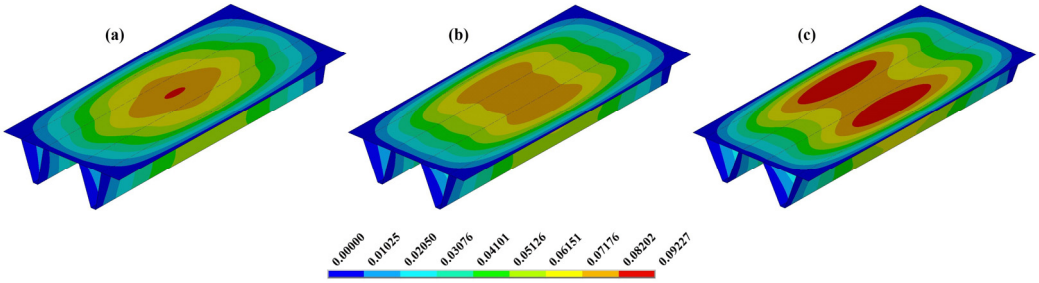


Figure 18. Strain distribution for plates with two hat-stiffeners, t_s = 4.75, and the following stiffener side-wall angles: (**a**) θ_s = 105°; (**b**) θ_s = 110°; and (**c**) θ_s = 115°.

In the plates with three, four, and five hat-stiffeners, presented in Figures 14–16, a total of 67, 70, and 73 geometric configurations were generated, respectively. In general, a more uniform structural behavior can be observed with respect to the maximum displacements induced by variations in the side-wall angles θ_s, compared to the single- and two-stiffener plates. The pattern already identified in certain thicknesses shown in Figures 12 and 13 is repeated: increasing θ_s causes a reduction in the maximum deflection up to a specific θ_s value for each thickness, after which further increases in θ_s lead to an increase in the maximum deflection. These θ_s values corresponding to the behavioral change points in the plates with three, four, and five hat-stiffeners, for thicknesses of 6.35 mm, 8.0 mm, and 9.53 mm, are the same as those found in the two-stiffener plates, indicating stability in the relationship between θ_s variation and the number of hat-stiffeners on the plate. Regarding the maximum deflections, in the three- and four-stiffener plates, all geometric configurations exhibited maximum deflections below those of the reference plate. In the three-stiffener plates, the best result was obtained using a thickness of t_s = 4.75 mm with a side-wall angle of θ_s = 130°, representing a reduction of 83.32% in the maximum deflection compared to the reference plate. For the four- and five-stiffener plates, the best result was also obtained with t_s = 4.75 mm; however, at θ_s = 125°, these configurations represent improvements of 77.94% and 70.27% in the maximum deflection relative to the reference plate, respectively. To illustrate, Figure 19 presents the strain distributions for the four-stiffener plates, considering the smallest thickness, t_s = 4.75 mm, and the largest thickness, t_s = 12.75 mm. Side-wall angles of θ_s = 90°, θ_s = 110°, and θ_s = 135° were adopted for both thicknesses.

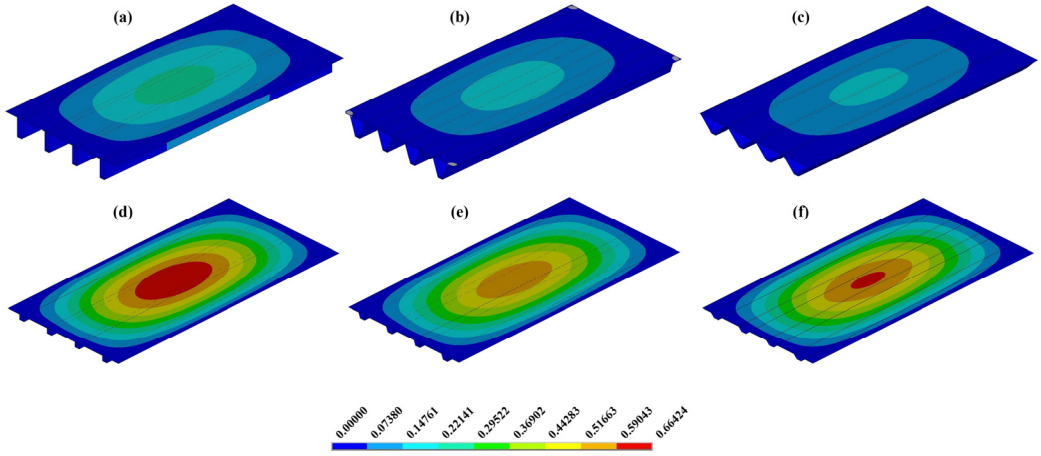


Figure 19. Strain distribution for plates with four hat-stiffeners, t_s = 4.75 mm, and (**a**) θ_s = 90°, (**b**) θ_s = 110°, and (**c**) θ_s = 135° and with t_s = 12.75 mm and (**d**) θ_s = 90°, (**e**) θ_s = 110°, and (**f**) θ_s = 135°.

From Figure 19 it can be observed that when keeping the total steel volume constant, the use of thicker hat-stiffeners requires a reduction in their height. As a result,

these configurations (Figure 19d–f) exhibit a displacement pattern more similar to that of the plate without stiffeners (reference plate). Conversely, when smaller thicknesses are adopted for the hat-stiffeners (Figure 19a–c), their height increases along with their moment of inertia, which enhances structural rigidity and explains the superior performance of these configurations.

4.3. Comparison with Results Reported by Alves et al. [22]

As mentioned earlier, Alves et al. [22] also studied plates with longitudinal hat-stiffeners. The methodology employed was similar to that used in the present study: the application of the Constructal Design method combined with the exhaustive search technique, the conversion of 30% of the plate volume into longitudinal stiffeners, and FEM simulation using the SHELL281 finite element. The applied loading, boundary conditions, and reference plate dimensions were also the same as those adopted in this study. The difference between the methodologies is that Alves et al. [22] fixed the side-wall angle at $\theta_s = 120^\circ$ and defined height levels, allowing the minor and major base dimensions to vary. The similarities in the employed methodology allow for a comparison between the best results obtained in both studies.

In the study conducted by Alves et al. [22], relative differences with respect to the reference plate in improving the mechanical behavior (i.e., reducing the maximum displacement) were reported as −86.26%, −80.20%, −82.17%, −76.34%, and −67.61% for hat-stiffened plates with one to five stiffeners, respectively. When the results of the present study (see Table 2) are compared with those of Alves et al. [22], additional improvements of approximately 7.5%, 8.5%, 1.0%, 1.5%, and 2.5% are observed. Therefore, particularly for one- and two-stiffener plates, the effect of the side-wall inclination proves to be a relevant design parameter.

4.4. The Study of the Moment of Inertia of the Geometries Found

As shown in Table 2, the structure's moment of inertia appears to be correlated with the magnitude of the maximum deflections observed. It can be seen in this direct comparison that the smallest deflections were obtained in geometric configurations that provided the highest moments of inertia. As the moment of inertia decreases, the deflections increase. This pattern is not observed in the case with a single stiffener, where the largest deflection occurred in a geometric configuration with a higher moment of inertia than those with multiple stiffeners. However, as illustrated in Figure 20, this geometric configuration compromised the stiffness provided by the stiffener, causing the plate with the added stiffener to behave similarly to the reference plate, albeit with a reduced thickness (due to the volume redistributed to form the stiffener), resulting in larger deflections.

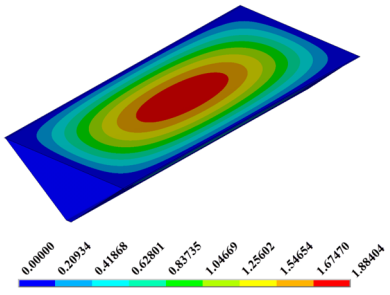


Figure 20. Geometric configuration obtained using a single stiffener, side-wall angle $\theta_s = 140^\circ$, and thickness $t_s = 4.75$ mm.

Regarding the structure's moment of inertia, it can be observed that, except in cases such as the one mentioned above, where the geometric configuration compromises the

stiffener's effectiveness, one of the fundamental parameters for increasing the structure's stiffness is the stiffener height. Increasing the height tends to shift the structure's centroid upward, enhancing the contribution of both the smaller base and the plate to the overall stiffness. This characteristic is evidenced by the fact that the largest moments of inertia were obtained in geometric configurations that produced stiffeners with the greatest heights.

However, a higher moment of inertia alone does not necessarily guarantee improved mechanical performance in terms of reducing the maximum out-of-plane displacement. The best geometries were observed to combine relatively high moments of inertia (though not always the highest) with a geometric configuration that promotes a more uniform distribution of displacements.

5. Conclusions

This study investigated the influence of the variation in the inclination angle of the side-walls of hat-stiffeners on the structural efficiency of stiffened steel plates. For this purpose, the Constructal Design method, combined with an exhaustive search technique, was employed, generating 336 geometric configurations that were analyzed using the FEM through ANSYS software. The stiffeners were longitudinally inserted, and the plates were considered simply supported under a uniformly distributed load of 10 kPa.

Considering that the primary purpose of using stiffeners in plates is to reduce deflection and improve the stiffness-to-weight ratio, the main objective of this work was to minimize displacements in plates with hat-stiffeners. The results showed that the majority of geometric configurations reduced displacements to below those obtained for the reference plate. The best performance was observed in the case of a single stiffener using a plate with thickness t_s = 4.75 mm and side-wall angle θ_s = 105°, leading to a 93.72% reduction in the maximum deflection compared to the reference plate (with no stiffeners but with the same amount of steel). This significant reduction highlights the importance of the strategic development of stiffeners focused on application.

The main scientific contributions of this work can be highlighted as follows:

- The application of the Constructal Design method together with exhaustive search proved to be an important tool for the evaluation and optimization of structures. While Constructal Design generates the search space (possible geometric configurations given the constraints and degrees of freedom), exhaustive search identifies the geometry that yields the best performance.
- The inclination angle of the side-wall of the hat-stiffener can influence its performance. Alves et al. [22] adopted θ_s = 120° and defined height levels. This difference allowed for a direct comparison of the results. The investigation developed in the present work identified a geometry that achieved an approximate 7.5% improvement over the best result obtained by Alves et al. [22] relative to the reference plate.
- The moment of inertia of the structure also strongly influences its performance regarding maximum displacements. Configurations exhibiting larger moments of inertia presented smaller deflections and taller stiffeners.
- Stiffener height emerges as an important parameter, since it shifts the structure's centroid upward, enhancing the contribution of the minor base and the plate to the overall structural stiffness.
- A higher moment of inertia alone does not guarantee the best mechanical performance; while a sufficiently high value is important, other geometric characteristics of the hat-stiffened plate also play a crucial role in determining its overall behavior.
- The ideal combination of these factors leads to superior performance by promoting a more uniform distribution of displacements, which is in agreement with the Constructal principle.

The following applied results are noteworthy:

- A significant increase in the mechanical resistance of steel plates was obtained by converting 30% of their volume into stiffeners. In this study, the improvement corresponded to a 93.72% reduction in the maximum deflections.
- Increasing the resistance to deflection of plates without increasing the amount of material can lead to cost reduction.

Future research could expand these findings and further improve the results by investigating different loading types, boundary conditions, plate aspect ratios, hat-stiffener orientations, alternative volumetric fractions to be converted into hat-stiffeners, and variations in side-wall angles associated with other parameters.

Author Contributions: Conceptualization, G.G.M., M.A.A. and L.A.I.; methodology, G.G.M., M.A.A. and L.A.I.; software, G.G.M., M.A.A. and L.A.I.; validation, G.G.M. and M.A.A.; formal analysis, L.A.O.R., E.D.d.S., W.R.A. and L.A.I.; investigation, L.A.O.R., E.D.d.S., W.R.A. and L.A.I.; resources, L.A.O.R., E.D.d.S. and L.A.I.; data curation, G.G.M., W.R.A. and L.A.I.; writing—original draft preparation, W.R.A. and L.A.I.; writing—review and editing, L.A.O.R., E.D.d.S., W.R.A. and L.A.I.; visualization, L.A.O.R., E.D.d.S., W.R.A. and L.A.I.; supervision, L.A.I.; project administration, L.A.I.; funding acquisition, L.A.O.R., E.D.d.S. and L.A.I. All authors have read and agreed to the published version of the manuscript.

Funding: This research was funded by Coordination for the Improvement of Higher Education Personnel—CAPES, funding code 001—and National Council for Scientific and Technological Development—CNPq, grant numbers: 307791/2019-0, 308396/2021-9, and 309648/2021-1.

Institutional Review Board Statement: Not applicable.

Informed Consent Statement: Not applicable.

Data Availability Statement: The original contributions presented in this study are included in the article. Further inquiries can be directed to the corresponding author.

Acknowledgments: The authors acknowledge the financial support for conducting this research provided by CAPES and CNPq.

Conflicts of Interest: The authors declare no conflicts of interest, and the funders had no role in the design of the study; in the collection, analyses, or interpretation of data; in the writing of the manuscript; or in the decision to publish the results.

Appendix A

This appendix presents all the geometric configurations generated through the search space of the Constructal Design method. Tables A1–A5 show the configurations based on the number of stiffeners in each plate, the variation in the side-wall angle θ_s, the thickness of the plate t_s, and the obtained height h_s. Subsequently, the maximum displacement is presented, and the relative percentage difference (RD) between the maximum deflection of the stiffened plate and that of the reference plate, without stiffeners, is provided. Finally, the moment of inertia related to the x-axis is indicated.

Table A1. Plates with a single hat-stiffener.

θ_s (mm)	t_s (mm)	y' (mm)	h_s (mm)	U_z^{max} (mm)	RD (%) U_z^{max}	I_x (mm^4)
90	4.75	0	611.5789	0.0778	−88.85	4.82×10^9
95	4.75	53.3026	609.2517	0.0654	−90.63	5.02×10^9
100	4.75	106.1996	602.2877	0.0471	−93.25	5.10×10^9
105	4.75	158.2883	590.7399	0.0438	−93.72	5.06×10^9
110	4.75	209.1723	574.6962	0.0863	−87.64	4.90×10^9
115	4.75	258.4644	554.2788	0.1549	−77.79	4.64×10^9
120	4.75	305.7895	529.6429	0.2580	−63.01	4.29×10^9
125	4.75	350.7873	500.9761	0.4166	−40.27	3.86×10^9
130	4.75	393.1154	468.4967	0.6946	−0.43	3.37×10^9
135	4.75	432.4516	432.4516	1.2555	79.98	2.85×10^9
140	4.75	468.4967	393.1154	1.8840	170.08	2.33×10^9
90	6.35	0	452.4409	0.0830	−88.10	2.66×10^9
95	6.35	39.4328	450.7193	0.0739	−89.40	2.77×10^9
100	6.35	78.5655	445.5674	0.0610	−91.25	2.81×10^9
105	6.35	117.1003	437.0244	0.0489	−92.99	2.79×10^9
110	6.35	154.7439	425.1554	0.0537	−92.30	2.70×10^9
115	6.35	191.2098	410.0508	0.0842	−87.93	2.56×10^9
120	6.35	226.2205	391.8254	0.1288	−81.54	2.36×10^9
125	6.35	259.5095	370.6179	0.1900	−72.76	2.12×10^9
130	6.35	290.8234	346.5899	0.2728	−60.89	1.85×10^9
135	6.35	319.9241	319.9241	0.3851	−44.79	1.57×10^9
140	6.35	346.5899	290.8234	0.5409	−22.47	1.28×10^9
145	6.35	370.6179	259.5095	0.7559	8.37	9.95×10^8
90	8	0	355.0000	0.0899	−87.11	1.65×10^9
95	8	30.9403	353.6491	0.0827	−88.14	1.71×10^9
100	8	61.6451	349.6068	0.0733	−89.49	1.74×10^9
105	8	91.8808	342.9037	0.0643	−90.78	1.72×10^9
110	8	121.4172	333.5909	0.0576	−91.74	1.67×10^9
115	8	150.0295	321.7393	0.0699	−89.98	1.58×10^9
120	8	177.5000	307.4390	0.0950	−86.38	1.46×10^9
125	8	203.6196	290.7990	0.1295	−81.43	1.31×10^9
130	8	228.1896	271.9458	0.1750	−74.91	1.14×10^9
135	8	251.0229	251.0229	0.2329	−66.61	9.66×10^8
140	8	271.9458	228.1896	0.3098	−55.59	7.86×10^8
145	8	290.7990	203.6196	0.4076	−41.57	6.11×10^8
150	8	307.4390	177.5000	0.5321	−23.72	4.50×10^8
90	9.53	0	294.7954	0.0978	−85.98	1.14×10^9
95	9.53	25.6931	293.6736	0.0916	−86.87	1.19×10^9
100	9.53	51.1907	290.3168	0.0844	−87.91	1.20×10^9
105	9.53	76.2987	284.7505	0.0777	−88.86	1.19×10^9
110	9.53	100.8260	277.0170	0.0731	−89.52	1.15×10^9
115	9.53	124.5859	267.1754	0.0746	−89.30	1.09×10^9
120	9.53	147.3977	255.3003	0.0924	−86.76	1.01×10^9
125	9.53	169.0877	241.4822	0.1166	−83.29	9.04×10^8
130	9.53	189.4908	225.8264	0.1483	−78.74	7.88×10^8
135	9.53	208.4518	208.4518	0.1893	−72.86	6.65×10^8
140	9.53	225.8264	189.4908	0.2417	−65.35	5.41×10^8
145	9.53	241.4822	169.0877	0.3084	−55.79	4.20×10^8
150	9.53	255.3003	147.3977	0.3929	−43.68	3.09×10^8
90	12.7	0	216.2205	0.1188	−82.98	6.15×10^8
95	12.7	18.8449	215.3977	0.1138	−83.68	6.39×10^8
100	12.7	37.5463	212.9356	0.1096	−84.29	6.48×10^8

Table A1. *Cont.*

θ_s (mm)	t_s (mm)	y' (mm)	h_s (mm)	U_z^{max} (mm)	RD (%) U_z^{max}	I_x (mm^4)
105	12.7	55.9620	208.8529	0.1068	−84.69	6.42×10^8
110	12.7	73.9518	203.1808	0.1063	−84.76	6.21×10^8
115	12.7	91.3787	195.9623	0.1090	−84.38	5.86×10^8
120	12.7	108.1102	187.2524	0.1188	−82.97	5.40×10^8
125	12.7	124.0190	177.1174	0.1363	−80.46	4.84×10^8
130	12.7	138.9838	165.6345	0.1589	−77.22	4.21×10^8
135	12.7	152.8910	152.8910	0.1879	−73.07	3.55×10^8
140	12.7	165.6345	138.9838	0.2247	−67.79	2.87×10^8
145	12.7	177.1174	124.0190	0.2713	−61.11	2.22×10^8
150	12.7	187.2524	108.1102	0.3301	−52.68	1.63×10^8

Table A2. Plates with two hat-stiffeners.

θ_s (mm)	t_s (mm)	y' (mm)	h_s (mm)	U_z^{max} (mm)	RD (%) U_z^{max}	I_x (mm^4)
90	4.75	0	295.7895	0.1347	−80.69	1.22×10^9
95	4.75	25.7798	294.6639	0.1119	−83.96	1.27×10^9
100	4.75	51.3633	291.2958	0.0936	−86.59	1.29×10^9
105	4.75	76.5559	285.7107	0.0827	−88.14	1.28×10^9
110	4.75	101.1660	277.9512	0.0800	−88.53	1.24×10^9
115	4.75	125.0060	268.0763	0.0923	−86.77	1.17×10^9
120	4.75	147.8947	256.1612	0.1065	−84.74	1.08×10^9
125	4.75	169.6579	242.2966	0.1188	−82.96	9.70×10^8
130	4.75	190.1298	226.5879	0.1248	−82.11	8.46×10^8
135	4.75	209.1547	209.1547	0.1224	−82.45	7.14×10^8
140	4.75	226.5879	190.1298	0.1190	−82.94	5.80×10^8
90	6.35	0	216.2205	0.1755	−74.84	6.63×10^8
95	6.35	18.8449	215.3977	0.1525	−78.14	6.88×10^8
100	6.35	37.5463	212.9356	0.1346	−80.70	6.98×10^8
105	6.35	55.9620	208.8529	0.1236	−82.27	6.92×10^8
110	6.35	73.9518	203.1808	0.1174	−83.17	6.69×10^8
115	6.35	91.3787	195.9623	0.1147	−83.56	6.32×10^8
120	6.35	108.1102	187.2524	0.1210	−82.66	5.82×10^8
125	6.35	124.0190	177.1174	0.1308	−81.25	5.22×10^8
130	6.35	138.9838	165.6345	0.1407	−79.83	4.55×10^8
135	6.35	152.8910	152.8910	0.1500	−78.50	3.83×10^8
140	6.35	165.6345	138.9838	0.1589	−77.22	3.11×10^8
145	6.35	177.1174	124.0190	0.1691	−75.75	2.41×10^8
150	6.35	187.2524	108.1102	0.1846	−73.54	1.76×10^8
90	8	0	167.5000	0.2222	−68.15	4.02×10^8
95	8	14.5986	166.8626	0.2000	−71.34	4.17×10^8
100	8	29.0861	164.9553	0.1821	−73.90	4.23×10^8
105	8	43.3522	161.7926	0.1707	−75.53	4.19×10^8
110	8	57.2884	157.3985	0.1639	−76.51	4.05×10^8
115	8	70.7886	151.8066	0.1606	−76.97	3.82×10^8
120	8	83.7500	145.0593	0.1602	−77.03	3.51×10^8
125	8	96.0741	137.2080	0.1623	−76.73	3.15×10^8
130	8	107.6669	128.3124	0.1669	−76.08	2.73×10^8
135	8	118.4404	118.4404	0.1743	−75.01	2.30×10^8
140	8	128.3124	107.6669	0.1859	−73.36	1.86×10^8

Table A2. *Cont.*

θ_s (mm)	t_s (mm)	y' (mm)	h_s (mm)	U_z^{max} (mm)	RD (%) U_z^{max}	I_x (mm^4)
145	8	137.2080	96.0741	0.2029	−70.91	1.44×10^8
150	8	145.0593	83.7500	0.2294	−67.12	1.05×10^8
90	9.53	0	137.3977	0.2688	−61.46	2.72×10^8
95	9.53	11.9750	136.8749	0.2469	−64.61	2.82×10^8
100	9.53	23.8589	135.3103	0.2288	−67.20	2.86×10^8
105	9.53	35.5611	132.7160	0.2168	−68.92	2.83×10^8
110	9.53	46.9928	129.1116	0.2096	−69.96	2.73×10^8
115	9.53	58.0668	124.5246	0.2060	−70.47	2.57×10^8
120	9.53	68.6988	118.9899	0.2055	−70.54	2.37×10^8
125	9.53	78.8081	112.5496	0.2080	−70.19	2.12×10^8
130	9.53	88.3175	105.2527	0.2134	−69.40	1.84×10^8
135	9.53	97.1548	97.1548	0.2225	−68.10	1.54×10^8
140	9.53	105.2527	88.3175	0.2365	−66.09	1.24×10^8
145	9.53	112.5496	78.8081	0.2574	−63.10	9.55×10^7
150	9.53	118.9899	68.6988	0.2885	−58.65	6.92×10^7
85	12.7	−8.5509	97.7369	0.3937	−43.56	1.31×10^8
90	12.7	0	98.1102	0.3681	−47.23	1.39×10^8
95	12.7	8.5509	97.7369	0.3459	−50.42	1.44×10^8
100	12.7	17.0367	96.6197	0.3277	−53.02	1.46×10^8
105	12.7	25.3928	94.7672	0.3147	−54.89	1.44×10^8
110	12.7	33.5557	92.1935	0.3065	−56.07	1.39×10^8
115	12.7	41.4632	88.9181	0.3025	−56.63	1.30×10^8
120	12.7	49.0551	84.9660	0.3023	−56.66	1.19×10^8
125	12.7	56.2737	80.3672	0.3060	−56.13	1.06×10^8
130	12.7	63.0640	75.1568	0.3141	−54.98	9.20×10^7
135	12.7	69.3744	69.3744	0.3271	−53.11	7.67×10^7
140	12.7	75.1568	63.0640	0.3466	−50.31	6.14×10^7
145	12.7	80.3672	56.2737	0.3746	−46.30	4.68×10^7
150	12.7	84.9660	49.0551	0.4143	−40.61	3.35×10^7

Table A3. Plates with three hat-stiffeners.

θ_s (mm)	t_s (mm)	y' (mm)	h_s (mm)	U_z^{max} (mm)	RD (%) U_z^{max}	I_x (mm^4)
90	4.75	0	190.5263	0.1616	−76.83	5.50×10^8
95	4.75	16.6055	189.8013	0.1517	−78.26	5.72×10^8
100	4.75	33.0845	187.6318	0.1423	−79.60	5.80×10^8
105	4.75	49.3118	184.0343	0.1355	−80.58	5.75×10^8
110	4.75	65.1638	179.0362	0.1303	−81.33	5.56×10^8
115	4.75	80.5199	172.6755	0.1259	−81.96	5.26×10^8
120	4.75	95.2632	165.0006	0.1219	−82.53	4.84×10^8
125	4.75	109.2814	156.0700	0.1183	−83.04	4.34×10^8
130	4.75	122.4680	145.9516	0.1163	−83.32	3.78×10^8
135	4.75	134.7224	134.7224	0.1183	−83.05	3.18×10^8
85	6.35	−11.9822	136.9572	0.2568	−63.19	2.76×10^8
90	6.35	0	137.4803	0.2461	−64.72	2.93×10^8
95	6.35	11.9822	136.9572	0.2295	−67.10	3.04×10^8
100	6.35	23.8732	135.3917	0.2135	−69.39	3.08×10^8
105	6.35	35.5825	132.7958	0.2015	−71.11	3.05×10^8
110	6.35	47.0210	129.1892	0.1928	−72.36	2.95×10^8

Table A3. *Cont.*

θ_s (mm)	t_s (mm)	y' (mm)	h_s (mm)	U_z^{max} (mm)	RD (%) U_z^{max}	I_x (mm^4)
115	6.35	58.1017	124.5995	0.1867	−73.24	2.78×10^8
120	6.35	68.7402	119.0614	0.1828	−73.79	2.56×10^8
125	6.35	78.8555	112.6173	0.1815	−73.98	2.29×10^8
130	6.35	88.3706	105.3160	0.1833	−73.72	1.99×10^8
135	6.35	97.2133	97.2133	0.1893	−72.87	1.67×10^8
140	6.35	105.3160	88.3706	0.2009	−71.20	1.35×10^8
145	6.35	112.6173	78.8555	0.2209	−68.34	1.04×10^8
150	6.35	119.0614	68.7402	0.2530	−63.73	7.53×10^7
85	8	−9.1514	104.6004	0.3493	−49.93	1.64×10^8
90	8	0	105.0000	0.3306	−52.60	1.74×10^8
95	8	9.1514	104.6004	0.3090	−55.70	1.80×10^8
100	8	18.2331	103.4048	0.2884	−58.66	1.83×10^8
105	8	27.1760	101.4222	0.2724	−60.95	1.80×10^8
110	8	35.9121	98.6677	0.2608	−62.62	1.74×10^8
115	8	44.3749	95.1623	0.2529	−63.75	1.64×10^8
120	8	52.5000	90.9327	0.2487	−64.35	1.50×10^8
125	8	60.2255	86.0110	0.2483	−64.41	1.34×10^8
130	8	67.4927	80.4347	0.2521	−63.86	1.16×10^8
135	8	74.2462	74.2462	0.2613	−62.54	9.73×10^7
140	8	80.4347	67.4927	0.2772	−60.26	7.82×10^7
145	8	86.0110	60.2255	0.3022	−56.68	5.99×10^7
150	8	90.9327	52.5000	0.3394	−51.35	4.32×10^7
85	9.53	−7.4023	84.6086	0.4281	−38.63	1.09×10^8
90	9.53	0	84.9318	0.4031	−42.21	1.15×10^8
95	9.53	7.4023	84.6086	0.3781	−45.80	1.19×10^8
100	9.53	14.7483	83.6415	0.3552	−49.08	1.21×10^8
105	9.53	21.9820	82.0378	0.3369	−51.71	1.19×10^8
110	9.53	29.0484	79.8098	0.3235	−53.63	1.15×10^8
115	9.53	35.8937	76.9743	0.3146	−54.89	1.08×10^8
120	9.53	42.4659	73.5531	0.3102	−55.53	9.87×10^7
125	9.53	48.7149	69.5721	0.3104	−55.50	8.79×10^7
130	9.53	54.5931	65.0615	0.3157	−54.75	7.59×10^7
135	9.53	60.0558	60.0558	0.3270	−53.12	6.33×10^7
140	9.53	65.0615	54.5931	0.3457	−50.45	5.06×10^7
145	9.53	69.5721	48.7149	0.3737	−46.43	3.85×10^7
150	9.53	73.5531	42.4659	0.4138	−40.68	2.76×10^7
80	12.7	−10.2001	57.8478	0.6005	−13.91	4.84×10^7
85	12.7	−5.1195	58.5166	0.5636	−19.21	5.26×10^7
90	12.7	0	58.7402	0.5319	−23.75	5.56×10^7
95	12.7	5.1195	58.5166	0.5041	−27.74	5.74×10^7
100	12.7	10.2001	57.8478	0.4803	−31.15	5.79×10^7
105	12.7	15.2031	56.7386	0.4613	−33.87	5.70×10^7
110	12.7	20.0903	55.1977	0.4474	−35.86	5.47×10^7
115	12.7	24.8247	53.2367	0.4389	−37.09	5.13×10^7
120	12.7	29.3701	50.8705	0.4356	−37.56	4.67×10^7
125	12.7	33.6920	48.1171	0.4379	−37.23	4.14×10^7
130	12.7	37.7574	44.9976	0.4463	−36.03	3.55×10^7
135	12.7	41.5356	41.5356	0.4613	−33.87	2.93×10^7
140	12.7	44.9976	37.7574	0.4842	−30.59	2.32×10^7
145	12.7	48.1171	33.6920	0.5164	−25.98	1.74×10^7
150	12.7	50.8705	29.3701	0.5594	−19.81	1.22×10^7

Table A4. Plates with four hat-stiffeners.

θ_s (mm)	t_s (mm)	y' (mm)	h_s (mm)	U_z^{max} (mm)	RD (%) U_z^{max}	I_x (mm^4)
90	4.75	0	137.8947	0.2501	−64.15	3.08×10^8
95	4.75	12.0183	137.3700	0.2294	−67.11	3.20×10^8
100	4.75	23.9452	135.7998	0.2079	−70.20	3.25×10^8
105	4.75	35.6898	133.1961	0.1902	−72.73	3.22×10^8
110	4.75	47.1628	129.5787	0.1761	−74.75	3.11×10^8
115	4.75	58.2768	124.9751	0.1653	−76.31	2.94×10^8
120	4.75	68.9474	119.4203	0.1577	−77.39	2.70×10^8
125	4.75	79.0932	112.9568	0.1539	−77.94	2.42×10^8
130	4.75	88.6370	105.6335	0.1548	−77.81	2.10×10^8
135	4.75	97.5063	97.5063	0.1619	−76.79	1.76×10^8
85	6.35	−8.5509	97.7369	0.3779	−45.83	1.52×10^8
90	6.35	0	98.1102	0.3564	−48.91	1.61×10^8
95	6.35	8.5509	97.7369	0.3280	−52.98	1.67×10^8
100	6.35	17.0367	96.6197	0.3002	−56.97	1.69×10^8
105	6.35	25.3928	94.7672	0.2779	−60.16	1.67×10^8
110	6.35	33.5557	92.1935	0.2610	−62.58	1.61×10^8
115	6.35	41.4632	88.9181	0.2492	−64.28	1.52×10^8
120	6.35	49.0551	84.9660	0.2422	−65.28	1.40×10^8
125	6.35	56.2737	80.3672	0.2402	−65.57	1.25×10^8
130	6.35	63.0640	75.1568	0.2437	−65.07	1.08×10^8
135	6.35	69.3744	69.3744	0.2537	−63.63	9.02×10^7
140	6.35	75.1568	63.0640	0.2717	−61.05	7.25×10^7
145	6.35	80.3672	56.2737	0.3001	−56.97	5.55×10^7
150	6.35	84.9660	49.0551	0.3425	−50.90	4.00×10^7
80	8	−12.8066	72.6296	0.5194	−25.55	8.15×10^7
85	8	−6.4277	73.4694	0.4834	−30.70	8.85×10^7
90	8	0	73.7500	0.4524	−35.14	9.38×10^7
95	8	6.4277	73.4694	0.4206	−39.70	9.70×10^7
100	8	12.8066	72.6296	0.3912	−43.92	9.79×10^7
105	8	19.0879	71.2370	0.3673	−47.35	9.66×10^7
110	8	25.2240	69.3023	0.3496	−49.88	9.30×10^7
115	8	31.1681	66.8402	0.3378	−51.58	8.74×10^7
120	8	36.8750	63.8694	0.3318	−52.43	8.00×10^7
125	8	42.3013	60.4125	0.3317	−52.45	7.12×10^7
130	8	47.4056	56.4958	0.3381	−51.54	6.14×10^7
135	8	52.1491	52.1491	0.3515	−49.60	5.11×10^7
140	8	56.4958	47.4056	0.3736	−46.44	4.08×10^7
145	8	60.4125	42.3013	0.4062	−41.77	3.10×10^7
150	8	63.8694	36.8750	0.4515	−35.27	2.21×10^7
80	9.53	−10.1929	57.8071	0.6060	−13.13	5.28×10^7
85	9.53	−5.1159	58.4755	0.5657	−18.91	5.73×10^7
90	9.53	0	58.6988	0.5305	−23.96	6.06×10^7
95	9.53	5.1159	58.4755	0.4979	−28.63	6.25×10^7
100	9.53	10.1929	57.8071	0.4692	−32.74	6.30×10^7
105	9.53	15.1924	56.6987	0.4459	−36.07	6.21×10^7
110	9.53	20.0762	55.1589	0.4289	−38.52	5.96×10^7
115	9.53	24.8072	53.1992	0.4181	−40.07	5.59×10^7
120	9.53	29.3494	50.8347	0.4133	−40.76	5.10×10^7
125	9.53	33.6683	48.0833	0.4149	−40.52	4.53×10^7
130	9.53	37.7309	44.9659	0.4233	−39.33	3.89×10^7
135	9.53	41.5064	41.5064	0.4389	−37.08	3.22×10^7
140	9.53	44.9659	37.7309	0.4632	−33.61	2.56×10^7

Table A4. *Cont.*

θ_s (mm)	t_s (mm)	y' (mm)	h_s (mm)	U_z^{max} (mm)	RD (%) U_z^{max}	I_x (mm^4)
145	9.53	48.0833	33.6683	0.4973	−28.70	1.93×10^7
150	9.53	50.8347	29.3494	0.5430	−22.15	1.36×10^7
75	12.7	−10.1082	37.7243	0.7834	12.30	2.17×10^7
80	12.7	−6.7819	38.4618	0.7377	5.75	2.41×10^7
85	12.7	−3.4039	38.9065	0.6982	0.09	2.61×10^7
90	12.7	0	39.0551	0.6643	−4.78	2.75×10^7
95	12.7	3.4039	38.9065	0.6350	−8.97	2.83×10^7
100	12.7	6.7819	38.4618	0.6109	−12.42	2.84×10^7
105	12.7	10.1082	37.7243	0.5923	−15.09	2.79×10^7
110	12.7	13.3576	36.6998	0.5792	−16.98	2.67×10^7
115	12.7	16.5054	35.3960	0.5717	−18.04	2.48×10^7
120	12.7	19.5276	33.8227	0.5704	−18.24	2.25×10^7
125	12.7	22.4011	31.9921	0.5753	−17.53	1.98×10^7
130	12.7	25.1041	29.9180	0.5866	−15.91	1.69×10^7
135	12.7	27.6161	27.6161	0.6047	−13.32	1.38×10^7
140	12.7	29.9180	25.1041	0.6304	−9.63	1.08×10^7
145	12.7	31.9921	22.4011	0.6642	−4.78	8.01×10^6
150	12.7	33.8227	19.5276	0.7070	1.35	5.53×10^6

Table A5. Plates with five hat-stiffeners.

θ_s (mm)	t_s (mm)	y' (mm)	h_s (mm)	U_z^{max} (mm)	RD (%) U_z^{max}	I_x (mm^4)
85	4.75	−9.2660	105.9112	0.350849	−49.70	1.83×10^8
90	4.75	0	106.3158	0.335148	−51.96	1.95×10^8
95	4.75	9.2660	105.9112	0.3055	−56.20	2.02×10^8
100	4.75	18.4615	104.7006	0.2755	−60.51	2.05×10^8
105	4.75	27.5166	102.6932	0.2513	−63.98	2.02×10^8
110	4.75	36.3621	99.9042	0.2327	−66.65	1.96×10^8
115	4.75	44.9310	96.3548	0.2191	−68.59	1.84×10^8
120	4.75	53.1579	92.0722	0.2106	−69.81	1.69×10^8
125	4.75	60.9802	87.0888	0.2074	−70.27	1.51×10^8
130	4.75	68.3385	81.4426	0.2101	−69.88	1.31×10^8
135	4.75	75.1766	75.1766	0.2204	−68.41	1.10×10^8
80	6.35	−12.9347	73.3565	0.5189	−25.61	8.68×10^7
85	6.35	−6.4921	74.2047	0.4838	−30.64	9.44×10^7
90	6.35	0	74.4882	0.4529	−35.08	1.00×10^8
95	6.35	6.4921	74.2047	0.4176	−40.13	1.03×10^8
100	6.35	12.9347	73.3565	0.3842	−44.92	1.05×10^8
105	6.35	19.2790	71.9501	0.3572	−48.80	1.03×10^8
110	6.35	25.4765	69.9960	0.3371	−51.67	9.94×10^7
115	6.35	31.4801	67.5092	0.3235	−53.63	9.34×10^7
120	6.35	37.2441	64.5087	0.3161	−54.68	8.56×10^7
125	6.35	42.7247	61.0172	0.3150	−54.84	7.62×10^7
130	6.35	47.8801	57.0613	0.3207	−54.02	6.58×10^7
135	6.35	52.6711	52.6711	0.3340	−52.12	5.48×10^7
140	6.35	57.0613	47.8801	0.3563	−48.93	4.39×10^7
145	6.35	61.0172	42.7247	0.3896	−44.14	3.34×10^7
150	6.35	64.5087	37.2441	0.4368	−37.38	2.39×10^7
80	8	−9.5506	54.1644	0.6345	−9.04	4.95×10^7
85	8	−4.7936	54.7907	0.5919	−15.15	5.36×10^7

Table A5. *Cont.*

θ_s (mm)	t_s (mm)	y' (mm)	h_s (mm)	U_z^{max} (mm)	RD (%) U_z^{max}	I_x (mm^4)
90	8	0	55.0000	0.5539	−20.59	5.67×10^7
95	8	4.7936	54.7907	0.5179	−25.75	5.85×10^7
100	8	9.5506	54.1644	0.4859	−30.35	5.90×10^7
105	8	14.2350	53.1259	0.4599	−34.07	5.80×10^7
110	8	18.8111	51.6831	0.4406	−36.84	5.58×10^7
115	8	23.2440	49.8469	0.4282	−38.62	5.23×10^7
120	8	27.5000	47.6314	0.4223	−39.47	4.77×10^7
125	8	31.5467	45.0534	0.4230	−39.35	4.23×10^7
130	8	35.3533	42.1324	0.4310	−38.22	3.63×10^7
135	8	38.8909	38.8909	0.4465	−35.99	3.01×10^7
140	8	42.1324	35.3533	0.4706	−32.53	2.39×10^7
145	8	45.0534	31.5467	0.5046	−27.67	1.80×10^7
150	8	47.6314	27.5000	0.5498	−21.18	1.28×10^7
75	9.53	−11.1186	41.4953	0.7668	9.92	2.82×10^7
80	9.53	−7.4598	42.3064	0.7161	2.66	3.13×10^7
85	9.53	−3.7441	42.7956	0.6721	−3.65	3.38×10^7
90	9.53	0	42.9591	0.6335	−9.19	3.57×10^7
95	9.53	3.7441	42.7956	0.5992	−14.11	3.67×10^7
100	9.53	7.4598	42.3064	0.5698	−18.32	3.69×10^7
105	9.53	11.1186	41.4953	0.5463	−21.69	3.63×10^7
110	9.53	14.6929	40.3683	0.5290	−24.16	3.47×10^7
115	9.53	18.1553	38.9341	0.5181	−25.72	3.25×10^7
120	9.53	21.4795	37.2037	0.5137	−26.36	2.95×10^7
125	9.53	24.6403	35.1900	0.5159	−26.05	2.61×10^7
130	9.53	27.6136	32.9086	0.5248	−24.77	2.23×10^7
135	9.53	30.3767	30.3767	0.5408	−22.47	1.84×10^7
140	9.53	32.9086	27.6136	0.5647	−19.05	1.45×10^7
145	9.53	35.1900	24.6403	0.5971	−14.40	1.08×10^7
150	9.53	37.2037	21.4795	0.6387	−8.44	7.55×10^6
75	12.7	−7.0513	26.3158	0.8760	25.57	1.21×10^7
80	12.7	−4.7309	26.8302	0.8340	19.56	1.34×10^7
85	12.7	−2.3745	27.1404	0.7973	14.30	1.44×10^7
90	12.7	0	27.2441	0.7656	9.76	1.51×10^7
95	12.7	2.3745	27.1404	0.7388	5.90	1.55×10^7
100	12.7	4.7309	26.8302	0.7167	2.75	1.55×10^7
105	12.7	7.0513	26.3158	0.6998	0.31	1.52×10^7
110	12.7	9.3180	25.6011	0.6879	−1.38	1.45×10^7
115	12.7	11.5139	24.6915	0.6814	−2.32	1.34×10^7
120	12.7	13.6220	23.5941	0.6802	−2.50	1.21×10^7
125	12.7	15.6266	22.3171	0.6844	−1.88	1.06×10^7
130	12.7	17.5122	20.8702	0.6943	−0.47	8.93×10^6
135	12.7	19.2645	19.2645	0.7099	1.77	7.25×10^6
140	12.7	20.8702	17.5122	0.7315	4.86	5.62×10^6
145	12.7	22.3171	15.6266	0.7592	8.83	4.12×10^6
150	12.7	23.5941	13.6220	0.7930	13.68	2.83×10^6

References

1. Szilard, R. *Theories and Applications of Plate Analysis: Classical, Numerical and Engineering Methods*; Wiley: Hoboken, NJ, USA, 2004. [CrossRef]
2. Li, B.; Gong, Y.; Gao, Y.; Hou, M.; Li, L. Failure Analysis of Hat-Stringer-Stiffened Aircraft Composite Panels under Four-Point Bending Loading. *Materials* **2022**, *15*, 2430. [CrossRef] [PubMed]

3. Ventsel, E.; Krauthammer, T. *Thin Plates and Shells: Theory: Analysis, and Applications*; CRC Press: Boca Raton, FL, USA, 2001. [CrossRef]
4. Bedair, O.K. A Contribution to the Stability of Stiffened Plates under Uniform Compression. *Comput. Struct.* **1998**, *66*, 535–570. [CrossRef]
5. Wu, H.; Liew, A.; Van Mele, T.; Block, P. Analysis and Optimisation of a Rib-Stiffened Vaulted Floor for Dynamic Performance. *Eng. Struct.* **2020**, *213*, 110577. [CrossRef]
6. Lukas, I.; Timmers, R.; Lang, R. Eurocode-Based Design Proposal for Non-Continuously Stiffened Steel Panels Subjected to Uniform Compression. *J. Constr. Steel Res.* **2025**, *228*, 109423. [CrossRef]
7. Rodrigues, F.; Vellasco, P.C.G.d.S.; de Lima, L.R.O.; da Silva, A.T. Structural Assessment of Stainless Steel Stiffened Panels. *Structures* **2023**, *57*, 105162. [CrossRef]
8. Soares, S.C.R.; Silva, G.C.; Fonseca, E.M.M. Computational Methodology for the Development of Wrinkled Tubes by Plastic Deformation. *Appl. Sci.* **2024**, *14*, 11126. [CrossRef]
9. Gudmundsson, S. Aircraft Structural Layout. In *General Aviation Aircraft Design*; Butterworth-Heinemann: Oxford, UK, 2022; pp. 113–146.
10. Straffelini, G. Sheet Metal Forming Operations. In *Ductility and Formability of Metals*; Springer: Cham, Switzerland, 2023; pp. 377–404.
11. Starman, B.; Cafuta, G.; Mole, N. A Method for Simultaneous Optimization of Blank Shape and Forming Tool Geometry in Sheet Metal Forming Simulations. *Metals* **2021**, *11*, 544. [CrossRef]
12. Mithu, M.A.H.; Karim, M.A.; Taj, F.A.; Rahman, A. Predicting Springback in V-Bending: Effects of Load, Load Holding Time, and Heat Treatment on Common Sheet-Metal Forming Operations. *Mater. Today Commun.* **2025**, *43*, 111668. [CrossRef]
13. Shi, G.-J.; Ji, Y.-H.; Xu, J.-B.; Wang, D.-Y.; Xu, Z.-T. Experimental Study of Structural Failure and Ultimate Strength of GFRP Girder with Hat Stiffeners and Foams under Bending Load. *Mar. Struct.* **2024**, *96*, 103607. [CrossRef]
14. Gan, L.; Zong, Z.; Lin, J.; Chen, Y.; Xia, M.; Chen, L. Influence of U-Shaped Stiffeners on the Blast-Resistance Performance of Steel Plates. *J. Constr. Steel Res.* **2022**, *188*, 107046. [CrossRef]
15. Wang, R.; Ju, J.; Li, Y.; Cheng, S. Ultimate Strength Assessment of Randomly Pitted Stiffened Panels Considering Stiffener Corrosion. *J. Constr. Steel Res.* **2024**, *223*, 109060. [CrossRef]
16. Bejan, A. Constructal-Theory Network of Conducting Paths for Cooling a Heat Generating Volume. *Int. J. Heat Mass Transf.* **1997**, *40*, 799–816. [CrossRef]
17. Bejan, A. *Shape and Structure, from Engineering to Nature*; Cambridge University Press: New York, NY, USA, 2000. [CrossRef]
18. Bejan, A.; Lorente, S. *Design with Constructal Theory*; John Wiley & Sons: Hoboken, NJ, USA, 2008. [CrossRef]
19. Bejan, A.; Zane, J.P. *Design in Nature: How the Constructal Law Governs Evolution in Biology, Physics, Technology, and Social Organization*; Anchor Books: New York, NY, USA, 2013.
20. Bejan, A. *The Physics of Life: The Evolution of Everything*; St. Martin's Press: New York, NY, USA, 2024.
21. da Silveira, T.; Pinto, V.; Neufeld, J.P.; Pavlovic, A.; Rocha, L.; dos Santos, E.; Isoldi, L.A. Applicability Evidence of Constructal Design in Structural Engineering: Case Study of Biaxial Elasto-Plastic Buckling of Square Steel Plates with Elliptical Cutout. *J. Appl. Comput. Mech.* **2021**, *7*, 922–934. [CrossRef]
22. Alves, M.A.; Rodrigues, E.M.; Pinto, V.T.; Rocha, L.A.O.; dos Santos, E.D.; Isoldi, L.A. Numerical Simulation, Constructal Design, and Systematic Search Applied to the Geometrical Evaluation of Hat-Stiffened Plates under Bending. *Res. Eng. Struct. Mater.* **2025**, *11*, 1–19. [CrossRef]
23. Alves, M.A.; Rodrigues, E.M.; Rocha, L.A.O.; dos Santos, E.D.; Almeida, W.R.; Isoldi, L.A. Numerical and Geometrical Evaluation of Steel Plates with Transverse Hat-Stiffeners Under Bending. *Metals* **2025**, *15*, 647. [CrossRef]
24. Reis, A.H. Constructal Theory: From Engineering to Physics, and How Flow Systems Develop Shape and Structure. *Appl. Mech. Rev.* **2006**, *59*, 269–282. [CrossRef]
25. Dos Santos, E.D.; Isoldi, L.A.; Gomes, M.N.; Rocha, L.A.O. The Constructal Design Applied to Renewable Energy Systems. In *Sustainable Energy Technologies*; Rincón-Mejía, E., Heras, A., Eds.; CRC Press—Taylor and Francis: Boca Raton, FL, USA, 2017; pp. 63–87.
26. Troina, G.; Cunha, M.; Pinto, V.; Rocha, L.; dos Santos, E.; Fragassa, C.; Isoldi, L. Computational Modeling and Constructal Design Theory Applied to the Geometric Optimization of Thin Steel Plates with Stiffeners Subjected to Uniform Transverse Load. *Metals* **2020**, *10*, 220. [CrossRef]
27. Nogueira, C.M.; Pinto, V.T.; Rocha, L.A.O.; Santos, E.D.D.; Isoldi, L.A. Numerical Simulation and Constructal Design Applied to Plates with Different Heights of Traverse and Longitudinal Stiffeners. *Eng. Solid Mech.* **2021**, *9*, 221–238. [CrossRef]
28. Pinto, V.T.; Rocha, L.A.O.; Fragassa, C.; dos Santos, E.D.; Isoldi, L.A. Multiobjective Geometric Analysis of Stiffened Plates under Bending through Constructal Design Method. *J. Appl. Comput. Mech.* **2020**, *6*, 1438–1449. [CrossRef]

29. Kucharski, D.M.P.; Pinto, V.T.; Rocha, L.A.O.; dos Santos, E.D.; Fragassa, C.; Isoldi, L.A. Geometric analysis by Constructal Design of stiffened steel plates under bending with transverse I-shaped or T-shaped stiffeners. *Facta Univ. Ser. Mech. Eng.* **2022**, *20*, 617–632. [CrossRef]
30. Lima, J.P.S.; Cunha, M.L.; dos Santos, E.D.; Rocha, L.A.O.; Real, M.V.; Isoldi, L.A. Constructal Design for the ultimate buckling stress improvement of stiffened plates submitted to uniaxial compressive load. *Eng. Struct.* **2020**, *203*, 109883. [CrossRef]
31. Tharian, M.; Nandakumar, C.G. Superelement for Structural Analysis of Steel Bunkers. *SSRN J.* **2023**. [CrossRef]
32. Tharian, M.; Nandakumar, C.G. Hat stiffened plates for ship building. *IJAERD* **2014**, *4*, 43–52.
33. Pal, A.K.; Harry, N.N.; Upadhyay, R.; Kushwaha, Y.K. Static Analysis of hat stiffened plate: A parametric study. *Int. J. Res. Eng. Sci. Manag. (IJRESM)* **2018**, *1*, 128–131.
34. Virág, Z.; Szirbik, S. Modal Analysis of Optimized Trapezoidal Stiffened Plates under Lateral Pressure and Uniaxial Compression. *Appl. Mech.* **2021**, *2*, 681–693. [CrossRef]
35. Filippatos, A.; Markatos, D.; Tzortzinis, G.; Abhyankar, K.; Malefaki, S.; Gude, M.; Pantelakis, S. Sustainability-Driven Design of Aircraft Composite Components. *Aerospace* **2024**, *11*, 86. [CrossRef]
36. Raju; Prusty, B.G.; Kelly, D.W.; Lyons, D.; Peng, G.D. Top Hat Stiffeners: A Study on Keel Failures. *Ocean Eng.* **2010**, *37*, 1180–1192. [CrossRef]
37. Sun, Z.; Lei, Z.; Zou, J.; Bai, R.; Jiang, H.; Yan, C. Prediction of failure behavior of composite hat-stiffened panels under in-plane shear using artificial neural network. *Compos. Struct.* **2021**, *272*, 114238. [CrossRef]
38. Kumar, A.P.; Méndez, J.P.; Burela, R.G.; Bisagni, C.; Harursampath, D.; Ponnusami, S.A. Non-linear buckling analysis of delaminated hat-stringer panels using variational asymptotic method. *Compos. Struct.* **2024**, *345*, 118276. [CrossRef]
39. Kumar, K.C.N.; Chavadaki, S.; Shaikh, A.; Singh, D.P.; Avikal, S. Weight optimization of a hat-stiffened panel of a typical transport aircraft composite wing. *Mater. Today Proc.* **2020**, *26*, 471–474. [CrossRef]
40. Kumar, K.S.; Kumar, K.C.N.; Mandal, P.C. Finite element analysis of composite hat-stiffened panels subjected to edge compression load. *Jordan J. Civ. Eng.* **2020**, *14*, 235–248. Available online: https://jjce.just.edu.jo/Download.ashx?f=TPwTijWxts67XewIlzO%2bYusgpM1C4mdts%2b%2beETCq%2bh4%3d (accessed on 12 October 2025).
41. Kumar, S.; Kumar, R.; Mandal, S. Experimental and numerical investigation of composite hat-stiffened panels under axial compression. *Sādhanā* **2020**, *45*, 130. [CrossRef]
42. Kumar, S.; Suman, S.; Ranjan, A. A parametric study on composite panel subjected to compression load. *J. Inst. Eng. Ser. A* **2024**, *105*, 15–24. [CrossRef]
43. Wang, Z.; Wang, B.; Bao, R.; Chen, X.; Liang, Q.; Yu, F. Buckling and post-buckling analysis of composite hat stiffened panels under axial compression loads. *J. Phys. Conf. Ser.* **2023**, *2489*, 012013. [CrossRef]
44. Lei, A.; Zou, P.; Deng, F.; Chen, Y. Bending experimental study on composite single hat stiffener panel in different environments. In Proceedings of the 3rd International Conference on Advanced Electronic Materials, Computers and Software Engineering (AEMCSE 2020), Shenzhen, China, 24–26 April 2020; IEEE: Xi'an, China, 2020; pp. 625–629. [CrossRef]
45. Liu, L.; Guan, Z. Effects of the fillers on the interface strength of the hat-stiffened composite panel. *Polym. Polym. Compos.* **2023**, *31*, 1–13. [CrossRef]
46. Qiu, J. Equivalent stiffness calculation of composite hat-stiffened panels based on Classical Laminate Theory. *Vibroeng. Procedia* **2022**, *47*, 42–48. [CrossRef]
47. Kim, G.-H.; Choi, J.-H.; Kweon, J.-H. Manufacture and Performance Evaluation of the Composite Hat-Stiffened Panel. *Compos. Struct.* **2010**, *92*, 2276–2284. [CrossRef]
48. Jin, B.C.; Li, X.; Mier, R.; Pun, A.; Joshi, S.; Nutt, S. Parametric Modeling, Higher Order FEA and Experimental Investigation of Hat-Stiffened Composite Panels. *Compos. Struct.* **2015**, *128*, 207–220. [CrossRef]
49. Yetman, J.E.; Sobey, A.J.; Blake, J.I.R.; Shenoi, R.A. Investigation into Skin Stiffener Debonding of Top-Hat Stiffened Composite Structures. *Compos. Struct.* **2015**, *132*, 1168–1181. [CrossRef]
50. El Samrout, A.; Braydi, O.; Younes, R.; Trouchu, F.; Lafon, P. A New Hybrid Method to Solve the Multi-Objective Optimization Problem for a Composite Hat-Stiffened Panel. *Stud. Comput. Intell.* **2018**, *774*, 77–88. [CrossRef]
51. Ram Murthy, V.; Annamalai, K.; Elango, M. Numerical Analysis of Hat Stiffened Composite Panels for Pre and Post Buckling Conditions. *IOP Conf. Ser. Mater. Sci. Eng.* **2021**, *1128*, 012021. [CrossRef]
52. Shi, M.; Chen, P. Simulation of manufacture of the hat-stiffened composite plate based on multidisciplinary coupling. *Acta Mater. Compos. Sin.* **2021**, *38*, 4150–4160. [CrossRef]
53. Wang, T.; Bai, R.; Wei, C.; Huang, X.; Bai, H. Interface Damage Analysis of Composite Hat-Stiffened Panels. *J. Phys. Conf. Ser.* **2021**, *1948*, 012139. [CrossRef]
54. Wang, Z.; Liu, K.; Yu, T.; Zong, S.; Wang, X. Structural Deformation Mechanism of the Hat-Stiffened Plate Used in Marine Structures under Impact Load. *Ocean Eng.* **2022**, *266*, 112736. [CrossRef]
55. Hochster, H.; Ranatunga, V.; Shemesh, N.N.; Haj-Ali, R. Surrogate PHFGMC Micromechanical Models for Multiscale Analysis: AI-Enhanced Low-Velocity Impact Analysis of Hat-Stiffened Composite Panels. *J. Compos. Mater.* **2024**, *59*, 305–320. [CrossRef]

56. Liu, B.; Zhang, L.; Liu, A.; Guedes Soares, C. Integrated Design Method of Marine C/GFRP Hat-Stiffened Panels towards Ultimate Strength Optimisation. *Ocean Eng.* **2025**, *317*, 120052. [CrossRef]
57. Yang, X.; Li, G.; Sun, C.; Niu, S.; Yang, Y.; Liu, X.; Shao, C. The Influence of High Toughness Resin Region on the Pull-off Failure Process of Hat-Stiffened Composite Structures. *Eng. Fail. Anal.* **2025**, *169*, 109214. [CrossRef]
58. *ASTM A36/A36M*; Standard Specification for Carbon Structural Steel. ASTM International: West Conshohocken, PA, USA, 2019.
59. ANSYS, Inc. *Element Reference—Release 2021 R2. Southpointe, 2600 ANSYS Drive*; ANSYS, Inc.: Canonsburg, PA, USA, 2021; Available online: https://pt.scribd.com/document/665578059/Ansys-Mechanical-APDL-Theory-Reference (accessed on 12 October 2025).
60. Zienkiewicz, O.C. *The Finite Element Method*; McGraw-Hill: London, UK, 1986.
61. Moaveni, S. *Finite Element Analysis: Theory and Application with ANSYS*, 3rd ed.; Pearson Prentice Hall: Hoboken, NJ, USA, 2008.
62. *JIS G 3101*; Rolled Steels for General Structure. Japanese Standards Association (JSA): Tokyo, Japan, 2015.
63. American Institute of Steel Construction (AISC). *Steel Construction Manual*, 15th ed.; American Institute of Steel Construction: Chicago, IL, USA, 2017; Table 2-1.
64. Carrijo, E.C.; Paiva, J.B.; Giogo, J.S. A numerical and experimental study of stiffened plates in bending. *TOMACS* **1999**, *21*, 12–18.

Disclaimer/Publisher's Note: The statements, opinions and data contained in all publications are solely those of the individual author(s) and contributor(s) and not of MDPI and/or the editor(s). MDPI and/or the editor(s) disclaim responsibility for any injury to people or property resulting from any ideas, methods, instructions or products referred to in the content.